A&A manuscript no.
(will be inserted by hand later)

Your thesaurus codes are:
06 (02.01.2; 02.08.1; 02.09.1; 02.19.1; 08.02.1; 13.25.5)

ASTRONOMY
AND
ASTROPHYSICS
29.4.1996

An analytic study of Bondi–Hoyle–Lyttleton accretion

I. Stationary flows

T. Foglizzo and M. Ruffert

Max–Planck–Institut für Astrophysik, Karl–Schwarzschild–Str. 1, Postfach 15 23, 85740 Garching, Germany

April 26, 1996

Abstract. We prove that the sonic surface of axisymmetric meridional stationary flows is always attached to the accretor, however small, if the adiabatic index of the gas is $\gamma = 5/3$.
Using local expansions near a point-like accretor, we extend Bondi's classification of spherically symmetric flows to axisymmetric flows, introducing the possibility of angular sectors reached by no flow lines, and singular directions of infinite mass flux, in addition to the angular regions of subsonic and supersonic accretion. For $\gamma < 5/3$, we show the impossibility of subsonic accretion onto a point–like accretor when the entropy of the flow is not uniform. The special case $\gamma = 5/3$ is treated separately.
We analyse the influence of the adiabatic index and Mach number of the flow at infinity on the mass accretion rate of shocked spherical flows. We propose an interpolation formula for the mass accretion rate of axisymmetric flows as a function of the Mach number and the adiabatic index, in the range $9/7 < \gamma < 5/3$.

Key words: Accretion, accretion disks – Hydrodynamics – Instabilities – Shock waves – Binaries: close – X-rays: stars

1. Introduction

Numerical simulations of the Bondi–Hoyle–Lyttleton (hereafter BHL) accretion flow, in 2–D and 3–D, have not only enabled the determination of the mean rate of accretion of mass, linear and angular momentum, but have also significantly modified our understanding of its dynamics. They have revealed that the accretion column foreseen by Hoyle & Lyttleton (1939) widens to form a detached bow shock if the adiabatic index of the accreted gas is $\gamma = 5/3$ (Hunt 1971) or $\gamma = 4/3$ (Hunt 1979). The shock structure observed in simulations was used by Eadie et al. (1975) to interpret the X–ray observations of Vel X-1.
Real situations like wind accretion in X-ray binaries require taking into account the density and velocity gradients in the incoming flow (see Ishii et al. 1993 and references therein), the effects of rotation (see Theuns et al. 1996 and references therein) as well as the intricacies of radiative transfer (see an overview in Blondin 1994). For the sake of a better understanding, we restrict our present investigation to the axisymmetric meridional accretion of a gas with uniform adiabatic index onto a gravitating accretor with constant velocity.
Although this configuration is highly simplified, a completely unexpected non–axisymmetric instability was discovered in numerical simulations for supersonic flows (Fryxell & Taam 1988). This instability could explain the observed variability of the radio or X-ray luminosity in some astrophysical systems (e.g. Ruffert & Melia 1994).
However, its is not easy to establish the consistency of the results of the few published 3–D numerical simulations which depend on the details of the numerical method: no instability appeared in the 3–D SPH simulations by Boffin (1991) whereas it was observed in the 3–D Eulerian simulations by Matsuda et al. (1992 and references therein) and Ruffert (1995 and references therein). Dome–shaped structures frequently appeared with Roe's method (approximate Riemann solver) of Matsuda et al. (1991), but not in the nested grid Piecewise Parabolic Method (PPM) of Ruffert (1991). Since numerical viscosity appears to play an important role, a sufficient resolution of the simulation is crucial. In this respect, numerical simulations encounter the following difficulty: the smallness of the accretor in simulations is limited by the computational power, because the shortest timestep of the simulation is usually determined by the region of high velocities in the vicinity of the accretor. The ratio of scales between the accretion radius and the radius $r_\star$ of a compact star, moving with a supersonic velocity v is typically of order:

$$\frac{r_{\rm A}}{r_\star} \sim 10^5 \left(\frac{10^3 {\rm kms}^{-1}}{v}\right)^2 \left(\frac{r_{\rm Schw.}}{r_\star}\right) , \tag{1}$$

where $r_{\rm Schw.}$ is the Schwarzschild radius. Note that in the case of accretion onto a neutron star, the relevant accretor boundary is the boundary of its magnetosphere, typically a factor $10-100$ larger than the Schwarzschild radius. Some of the most recent

Send offprint requests to: foglizzo@saclay.cea.fr

3–D simulations (Ruffert 1992, 1994a) could allow a ratio up to $r_{\mathrm{A}}/r_{\star} \sim 10^2$ (the full domain of the simulation extends up to $\sim$ 16 accretion radii), by using a PPM code with multiple nested grids. Such an accreting sphere is still more than 100 times larger than $r_{\mathrm{Schw.}}$, and typically 10 times larger than the magnetosphere of a neutron star. One would like to be able to predict, on an analytical basis, which changes are likely to occur if the size of the accretor is further decreased. The role of the boundary conditions at the surface of the accretor is closely related to the position of the sonic surface, and we shall use analytical arguments to obtain some insights on this question.

An analytical description of axisymmetric stationary flows is also a first step towards the analysis of their stability, which we postpone to a future paper. Bisnovatyi-Kogan et al. (1979) found self-similar stationary solutions, and one would like to know to what extent any generic stationary solution would behave in the same way as their solution. More generality is gained by studying, in the same spirit as Theuns & David (1992) for the spherical case, the first order behaviour of all quantities near the accretor for an axisymmetric flow, and in particular their departure from sphericity.

Some analytic formulae have been proposed to fit the mass accretion rate observed in simulations (Hunt 1979; Ruffert 1994b), but none of them filled the gap between the well studied cases of axisymmetric accretion of dust (Hoyle & Lyttleton 1939; Bondi & Hoyle 1944) on the one hand, and spherical accretion of a gas (Bondi 1952) on the other, for an arbitrary value of the adiabatic index . Continuing in this direction, we add to these reference models the spherical accretion of a shocked gas with uniform adiabatic index, in order to see the effect of both the kinetic and the thermal energies, and extend this approach to axisymmetric meridional stationary flows.

We first recall in Sect. 2 the general equations governing a stationary flow and formulate the axisymmetric problem with a single equation in cylindrical coordinates. The shape of the sonic surface is analysed in Sect. 3. We establish some properties of the flow by performing local expansions in the vicinity of the accretor in Sect. 4. We present in Sect. 5 the analytical solution of the spherical accretion from a gas with constant kinetic and thermal energies at infinity. An interpolation formula for the mass accretion rate of axisymmetric meridional flows is proposed in Sect. 6. We summarize our conclusions in Sect. 7.

2. Equations of a stationary flow in a gravitational potential

2.1. General equations

The continuity equation for a gas of velocity $\boldsymbol{v}$ and density ρ is:

$$\nabla \cdot (\rho \boldsymbol{v}) = 0 \ . \tag{2}$$

We restrict our study to the case of a gas of uniform adiabatic index $1 < \gamma < 5/3$. The entropy S of a gas with pressure P is defined as:

$$S \equiv \frac{\mathcal{R}}{(\gamma-1)\mu} \log \frac{P}{\rho^\gamma} \ , \tag{3}$$

in which $\mathcal{R}$ is the gas constant and μ is the mean molecular weight. The entropy is constant along each flow line ($\boldsymbol{v} \cdot \nabla S = 0$), except when matter passes through a shock.
The temperature T and the square of the sound velocity c^2 are simply related through a multiplicative constant:

$$c^2 \equiv \frac{\gamma P}{\rho} = \frac{\gamma \mathcal{R} T}{\mu} \ . \tag{4}$$

For the sake of simplicity, we shall set the ratio $\mathcal{R}/\mu = 1$ everywhere in what follows. Since the mean molecular weight is constant throughout our study, this convention is equivalent to changing the units of temperature and entropy, without loosing any generality.
Using Eq. (3), the pressure force can be written as:

$$\frac{\nabla P}{\rho} = \frac{1}{\gamma-1} \nabla c^2 - T \nabla S \ . \tag{5}$$

The Euler equation for a stationary flow with velocity $\boldsymbol{v}$ around an accretor of mass M is then:

$$\nabla \frac{v^2}{2} + (\nabla \times \boldsymbol{v}) \times \boldsymbol{v} = \nabla \frac{GM}{r} - \frac{1}{\gamma-1} \nabla c^2 + T \nabla S \ , \tag{6}$$

in which r is the distance to the centre of the accretor and G is the gravitational constant.
The Bernoulli equation is obtained by integrating the Euler equation along a flow line. It states that the quantity B

$$B \equiv \frac{v^2}{2} + \frac{c^2}{\gamma-1} - \frac{GM}{r} \ , \tag{7}$$

is constant along each flow line. The three terms of this sum are respectively the kinetic, the thermal, and the gravitational energies.
The vorticity of the flow is simply defined as

$$\boldsymbol{w} \equiv \nabla \times \boldsymbol{v} \ . \tag{8}$$

By using the definition of the Bernoulli constant (7) in the Euler equation (6), we obtain the following equation for any stationary flow,

$$\boldsymbol{w} \times \boldsymbol{v} = T \nabla S - \nabla B \ . \tag{9}$$

This formula is particularly useful because it expresses the vorticity in terms of invariant quantities B and S.
The Bernoulli constant B remains constant along a flow line, even through a shock. By contrast, the entropy S increases through a shock.
In the classic BHL case of a flow with constant and uniform

velocity at infinity, the Bernoulli constant is uniformly constant ($\boldsymbol{\nabla} B = \mathbf{o}$), and so does not contribute to the vorticity:

$$\boldsymbol{w} \times \boldsymbol{v} = T \boldsymbol{\nabla} S \ . \tag{10}$$

If, in addition, the flow is isentropic at infinity, the only possible source of vorticity gradients is the shock front. Note that Eq. (10) implies the conservation of entropy ($\boldsymbol{v} \cdot \boldsymbol{\nabla} S = 0$). Thus the only remaining differential equations are the continuity Eq. (2) and the vorticity Eq. (10).

2.2. Third–order partial differential system of an axisymmetric stationary flow in cylindrical coordinates

We consider the axisymmetric stationary flow of a gas with uniform density and constant velocity $\boldsymbol{v}_\infty \parallel \boldsymbol{x}$ with respect to the accretor. The geometry of the flow lines is described by a single function, the angle $\beta(r, \theta)$ between the radial direction and the flow line, defined by:

$$\tan\beta \equiv \frac{v_\theta}{v_r} \ . \tag{11}$$

We define by $\boldsymbol{n}$ the direction perpendicular to the velocity, in the plane containing the symmetry axis. Denoting by $\boldsymbol{e}_r, \boldsymbol{e}_\theta$ the unit vectors in cylindrical coordinates, we can write:

$$\boldsymbol{v} \equiv -v(\cos\beta \boldsymbol{e}_r + \sin\beta \boldsymbol{e}_\theta) \ , \tag{12}$$

$$\boldsymbol{n} \equiv \sin\beta \boldsymbol{e}_r - \cos\beta \boldsymbol{e}_\theta \ . \tag{13}$$

When useful throughout the paper, we denote by $\bar{r}$ the dimensionless distance normalized to the modified accretion radius $r_{\rm E}$, defined as:

$$r_{\rm E} \equiv \frac{GM}{B_\infty} = \frac{GM}{\frac{v_\infty^2}{2} + \frac{c_\infty^2}{\gamma - 1}} \ , \tag{14}$$

It coincides with the classic accretion radius $r_{\rm A}$ for large Mach numbers, when the kinetic energy largely exceeds the thermal energy:

$$r_{\rm A} \equiv \frac{2GM}{v_\infty^2} \ . \tag{15}$$

We shall denote distances normalized to $r_{\rm E}$ by a bar.
Using Eqs. (3) and (7), all relevant flow quantities can be rewritten as functions of $S, \mathcal{M}, \beta$:

$$\boldsymbol{v} = -\mathcal{M} \left[\frac{2B_\infty(1+\bar{r})}{\bar{r}\left(\mathcal{M}^2 + \frac{2}{\gamma-1}\right)} \right]^{\frac{1}{2}} (\cos\beta \boldsymbol{e}_r + \sin\beta \boldsymbol{e}_\theta) \ , \tag{16}$$

$$\rho = {\rm e}^{-S} \left[\frac{2B_\infty(1+\bar{r})}{\gamma\bar{r}\left(\mathcal{M}^2 + \frac{2}{\gamma-1}\right)} \right]^{\frac{1}{\gamma-1}} \ , \tag{17}$$

$$c = \left[\frac{2B_\infty(1+\bar{r})}{\bar{r}\left(\mathcal{M}^2 + \frac{2}{\gamma-1}\right)} \right]^{\frac{1}{2}} \ , \tag{18}$$

$$P = {\rm e}^{-S} \left[\frac{2B_\infty(1+\bar{r})}{\gamma\bar{r}\left(\mathcal{M}^2 + \frac{2}{\gamma-1}\right)} \right]^{\frac{\gamma}{\gamma-1}} \ . \tag{19}$$

The azimuthal component of the Euler Eq. (6), multiplied by r, is:

$$v_r \frac{\partial r v_\theta}{\partial r} + v_\theta \frac{\partial v_\theta}{\partial \theta} + \frac{1}{\rho}\frac{\partial P}{\partial \theta} = 0 \ . \tag{20}$$

We denote by w the third and only non-zero component of the vorticity vector:

$$w \equiv \frac{1}{r}\frac{\partial r v_\theta}{\partial r} - \frac{1}{r}\frac{\partial v_r}{\partial \theta} \ . \tag{21}$$

By combining the vectorial vorticity Eq. (10) and the scalar continuity Eq. (2), we obtain a third order differential system in terms of $\beta, \mathcal{M}^2, S$ only, with variables r, θ (see Appendix A). This system is hyperbolic in regions where $\mathcal{M} > 1$, and elliptic where $\mathcal{M} < 1$. It requires *three* functions $\beta_*(\theta), \mathcal{M}_*^2(\theta), S_*(\theta)$ as boundary conditions on the surface of the accretor. It should be noted that if the entropy is uniform, the flow is potential ($\boldsymbol{v} \equiv \boldsymbol{\nabla}\Phi_{\rm v}$), and the Bernoulli and the continuity equations provide a second order partial differential equation on $\Phi_{\rm v}(r, \theta)$. In this case, the boundary conditions at the surface of the accretor consist of *two* functions of θ, namely $\Phi_{\rm v}(r = r_\star, \theta)$ and its radial derivative.

2.3. Further reduction of the differential system

We can simplify the system by using the modified stream function introduced by Crocco (1936), defined as follows:

$$\frac{\partial \Psi}{\partial \theta} \equiv (2GM)^{-\frac{\gamma+1}{2(\gamma-1)}} c^{\frac{2}{\gamma-1}} r^2 v_r \sin\theta < 0 \ , \tag{22}$$

$$\frac{\partial \Psi}{\partial \log r} \equiv -\tan\beta \frac{\partial \Psi}{\partial \theta} \ . \tag{23}$$

Where there is no shock, Ψ is conserved along flow lines (because $\boldsymbol{v} \cdot \boldsymbol{\nabla}\Psi = 0$). It is also conserved across shocks, since the derivatives of Ψ have only a finite discontinuity there. The entropy can be expressed as a function of Ψ, and thus becomes a function of a single variable $S(r, \theta) = S(\Psi(r, \theta))$, defined once and for all along the shock.
Let us index the flow lines with their distance ϖ to the symmetry axis (i.e. their impact parameter) at infinity. Only the gas within a cylinder of radius ϖ_0 is accreted, so that the total mass accretion rate is $\dot{M} = \pi\varpi_0^2 \rho_\infty v_\infty$. At infinity, the mass flux inside the cylinder of radius ϖ is directly proportional to $\Psi(\varpi)$ through the following product:

$$\pi\varpi^2 \rho_\infty v_\infty = \pi \left[\frac{(2GM)^{\frac{\gamma+1}{2}}}{\gamma} \right]^{\frac{1}{\gamma-1}} \Psi(\varpi) {\rm e}^{-S_\infty} \ . \tag{24}$$

For the sake of clarity of the equations, let us define:

$$\epsilon_\Psi \equiv \bar{r} \frac{\partial \Psi}{\partial \bar{r}} \ . \tag{25}$$

Because the total mass accretion rate is finite, we deduce from Eq. (24) that Ψ is bounded in the vicinity of the accretor, and $\lim_{r \to 0} \epsilon_\Psi = 0$.

Using the definition of Ψ and the Bernoulli equation, we can formally write the Mach number $\mathcal{M}$ as a function of the gradient of Ψ through the following algebraic equation:

$$(r\nabla\Psi)^2 = \frac{\mathcal{M}^2 \sin^2\theta}{r^{\frac{5-3\gamma}{\gamma-1}}} \left[\frac{1+\bar{r}}{\mathcal{M}^2 + \frac{2}{\gamma-1}}\right]^{\frac{\gamma+1}{\gamma-1}} \quad . \tag{26}$$

At a given position (r, θ), the maximum of the right hand side term is reached at $\mathcal{M} = 1$. This defines a maximum value for the gradient of the stream function, i.e. for the local mass flux according to Eq. (24). For any value of $\nabla\Psi$ below this maximum, two Mach numbers are solutions of the Eq. (26). As for spherically symmetric flows classified by Bondi (1952), one solution is subsonic, while the other is supersonic.

Equation (26) can be derived with respect to r or θ to express the partial derivatives of $\mathcal{M}$ with respect to r or θ as function of $\mathcal{M}$ and the derivatives of Ψ. The vorticity Eq. (10) can therefore be expressed with derivatives of Ψ only, as follows:

$$\begin{aligned}
&\bar{r}^2 \frac{\partial^2\Psi}{\partial\bar{r}^2} \left\{1 + \frac{\mathcal{M}^2}{1-\mathcal{M}^2}\left(\frac{\epsilon_\Psi}{r\nabla\Psi}\right)^2\right\} \\
&+ \bar{r}\frac{\partial\Psi}{\partial\bar{r}} \left\{\frac{3}{2} + \frac{5-3\gamma}{2(\gamma-1)(1-\mathcal{M}^2)}\right. \\
&\qquad - \frac{\bar{r}}{1+\bar{r}}\left[\frac{2+(\gamma-1)\mathcal{M}^2}{2(\gamma-1)(1-\mathcal{M}^2)}\right] - \frac{\epsilon_\Psi S'(\Psi)}{\gamma\mathcal{M}^2} \\
&\qquad \left. + \frac{\mathcal{M}^2}{1-\mathcal{M}^2}\frac{1}{(r\nabla\Psi)^2}\left(\epsilon_\Psi^2 + 2\frac{\partial\epsilon_\Psi}{\partial\theta}\frac{\partial\Psi}{\partial\theta} + \epsilon_\Psi\frac{\partial^2\Psi}{\partial\theta^2}\right)\right\} \\
&+ \frac{1}{1-\mathcal{M}^2}\left(\frac{\partial^2\Psi}{\partial\theta^2} - \frac{1}{\tan\theta}\frac{\partial\Psi}{\partial\theta}\right) + \left(\frac{\partial\Psi}{\partial\theta}\right)^2 \frac{S'(\Psi)}{\gamma\mathcal{M}^2} = 0 \ .
\end{aligned} \tag{27}$$

This equation can be viewed as an explicit partial differential equation of second order on Ψ, with $\mathcal{M}$ implicitly depending on $\nabla\Psi$ through the algebraic Eq. (26). In an equivalent way, Eq. (27) can also be considered as a second order polynom in $\mathcal{M}^2$, whose two roots explicitly determine $\mathcal{M}^2$ as a function of Ψ and its derivatives. Inserting one of the two roots into Eq. (26), we obtain an implicit differential equation of second order containing explicitely only Ψ and its derivatives of first and second order.
This compact formulation will allow us to perform in Sect. 4 a direct analysis of the behaviour of the solution in the vicinity of $r = 0$.

3. The sonic surface of axisymmetric stationary flows

3.1. Three topologies of axisymmetric accretion

Numerical simulations of axisymmetric accretion with different Mach numbers, adiabatic indices and accretor sizes have exhibited three different topologies of the sonic surface. These three topologies are illustrated in Fig. 1.

- Type F (fast accretion): the sonic surface is detached from the accretor. This occurs for subsonic flows for small enough accretors (Ruffert 1994b, 1995, 1996).

Fig. 1. Three topologies of axisymmetric accretion. The sonic surface is represented as a dotted line. It touches the accretor at an angle θ_{so} with the symmetry axis for the types SF and FSF. For the type FSF, the solid line represents the shock surface reaching the accretor at an angle θ_{sh} with the symmetry axis.

- Type SF (mixed slow/fast accretion): the sonic surface reaches the surface of the accretor. It subtends an angle θ_{so} relative to the axis of symmetry at the position of the accretor. This is the case for subsonic flows with large accretors, and supersonic flows with $\gamma = 5/3$ (Matsuda et al. 1992; Ruffert & Arnett 1994; Ruffert 1994a).

- Type FSF (mixed fast/slow/fast accretion): both the sonic surface and the shock surface touch the surface of the accretor. They respectively subtend the angles θ_{so} and θ_{sh} relative to the axis of symmetry. This occurs for all supersonic flows when the accretor is large enough, for all the known supersonic 3–D simulations with γ close to one (Ishii et al. 1993; Ruffert 1996). More complicated topologies were observed by Hunt (1979) and Ruffert (1995) in simulations of supersonic flows with $\gamma = 4/3$, where the bow shock is linked to the accretor by a conical shock. These can also be classified as Type FSF, with the difference that the entropy in the supersonic flow ahead of the attached shock is not uniform.
The topology of the flow in numerical simulations appears to depend strongly on the size of the accretor: all the supersonic flows are of Type FSF if the accretor is big enough, but some become Type SF or F when the accretor size is decreased. In order to spare computing time, which increases with decreasing accretor size, one would like to use the largest accretor size leading to a physically relevant accretion process (cf. Eq. 1). Type F flows are numerically easier to handle, because unphysical effects due to a possible reflection of waves at the boundary of the too large accretor can be avoided.

3.2. The shape of the flow tubes at the sonic radius

Let us consider a flow tube of cross section Φ, parametrized along the tube by the curvilinear variable l. We denote by ΔS the entropy that this flow tube gains passing through a shock, and by ρ_∞ and c_∞ the density and the sound speed at large distances from the accretor, before the shock. The density ρ and sound speed c after the shock satisfy the following equation:

$$\mathrm{e}^{-\Delta S} \equiv \left(\frac{c_\infty}{c}\right)^{\frac{2}{\gamma-1}} \frac{\rho}{\rho_\infty} \ . \tag{28}$$

Using the Bernoulli equation (7) and the entropy equation (28), we can write the momentum as a function of the Mach number $\mathcal{M}$ and the position r:

$$\rho v = \frac{\mathcal{M}\rho_\infty}{c_\infty^{\frac{2}{\gamma-1}}} \mathrm{e}^{-\Delta S} \left[\frac{(\gamma-1)B_\infty\left(1+\frac{1}{\bar{r}}\right)}{1+\frac{\gamma-1}{2}\mathcal{M}^2}\right]^{\frac{\gamma+1}{2(\gamma-1)}} \ . \tag{29}$$

Fig. 2. The position of the sonic point depends on the shape of the flow tube: for an axisymmetric flow tube, it is shifted from the spherical position depending on whether its cross section increases faster or slower than the square of the distance to the accretor

The continuity equation (2) states that the mass flux is conserved along the flow tube:

$$\frac{\partial}{\partial l}(\rho v \Phi) = 0 \ . \tag{30}$$

By substituting Eq. (29) into Eq. (30), we obtain, along a given flow line:

$$\frac{\partial \log \Phi}{\partial \log r} = \frac{\gamma+1}{2(\gamma-1)}\frac{1}{1+\bar{r}} - \frac{1-\mathcal{M}^2}{2+(\gamma-1)\mathcal{M}^2}\frac{\partial \log \mathcal{M}^2}{\partial \log r} \ , \tag{31}$$

where the derivatives are calculated along a flow line, i.e. $\partial/\partial r \equiv (\partial/\partial l)(\partial l/\partial r)$. The regularity of $\partial\mathcal{M}/\partial l$ at the sonic point $\mathcal{M}(\bar{r}_{\rm so}) \equiv 1$ implies:

$$\frac{\partial \log \Phi}{\partial \log r} = 2 + 2\frac{r_0 - r_{\rm so}}{r_{\rm E} + r_{\rm so}} \ . \tag{32}$$

We have denoted by r_0 the radius of the sonic sphere in the spherical case:

$$r_0 \equiv \frac{5-3\gamma}{4}\frac{GM}{c_\infty^2 + \frac{\gamma-1}{2}v_\infty^2} \ . \tag{33}$$

It is remarkable that the spherical sonic radius is a function of the total energy B_∞ only, and is independent of the entropy of the flow.

The regularity condition (32) is a constraint on the shape of the flux tube at the sonic radius. Note that this condition is valid for any stationary flow, with no hypothesis on its symmetry. Let us illustrate it for an inflowing axisymmetric flow tube: the spherical case corresponds to radial flow lines, and thus to a conical flow tube. If the sonic radius is smaller than the spherical one, the cross section of the flow tube increases faster than the square of the distance to the accretor, thus the azimuthal component $v_\theta(r_{\rm so})$ of the velocity at the sonic radius must be oriented towards the axis of symmetry. Conversely, if the sonic radius is larger than the spherical one, the cross section of the flow tube increases more slowly than the square of the distance to the accretor, and $v_\theta(r_{\rm so})$ must be oriented away from the axis of symmetry (see Fig. 2).

3.3. A geometrical property of Type F flows

Fig. 3. If the sonic surface (dashed line) of the axisymmetric flow is detached from the accretor, it must intersect the sonic sphere (dotted line) of the equivalent spherically symmetric flow.

We prove in Appendix B the following property $\mathcal{P}$:
If the sonic surface is detached from the accretor, it must intersect at least once the sonic sphere of radius r_0 of the corresponding spherically symmetry flow with same energy.
r_0 is defined in Sect. 3.2 by Eq. (33). This property can be understood intuitively from Fig. 3, by using the geometrical interpretation of Eq. (32) in Sect. 3.2, in the simple case where the azimuthal velocity is of constant sign along the sonic surface in the interval $0 < \theta < \pi$. If the azimuthal velocity is directed away from the axis on one side of the accretor (for example, $r_{\rm so}(0) > r_0$), it will be oriented towards the axis on the other side ($r_{\rm so}(\pi) < r_0$), thus implying by continuity an intersection of the sonic surface with the sonic sphere. We show in Appendix B that this property is true for any axisymmetric flow, without any hypothesis on the distribution of azimuthal velocities.
Former studies of the BHL accretion have dealt with two set of length scales, one associated to the Hoyle-Lyttleton accretion of dust (the accretion radius $r_{\rm A}$), and the other associated to the spherical accretion (the Bondi radius $r_{\rm B}$ and the corresponding sonic radius $r_0(\mathcal{M}_\infty = 0)$). None of these scales took into account both the kinetic energy and the thermal energy of the gas. In particular, the significance of the sonic radius $r_0(\mathcal{M}_\infty = 0)$ for axisymmetric flows has always been dubious. The property $\mathcal{P}$ establishes the fundamental meaning of the spherical radius $r_0(\mathcal{M}_\infty)$, in relation with the sonic surface, for axisymmetric flows of Type F.
The geometrical property $\mathcal{P}$ is useful for numerical simulations of the BHL flow, in order to fix the maximum size of the totally absorbing accretor. As discussed in Sect. 3.1, since the sonic surface must cross the sonic sphere, the accretor size $r_\star$ should at least be smaller than the spherical sonic radius r_0. However, although the sonic sphere is larger than the accretor size used in numerical simulations with $\gamma = 4/3$ and $\gamma = 1.01$ (see Ruffert 1995, 1996), the sonic surface and the shock surface appear to be attached to the accretor. Although necessary, the condition $r_\star < r_0$ is far from being sufficient.

3.3.1. Consequence for flows with $\gamma = 5/3$

Since $r_0(\gamma = 5/3) = 0$, the sonic surface of flows with $\gamma = 5/3$ must always reach the surface of the accretor. Following the nomenclature introduced in Sect. 3.1, *the topology of the accretion with $\gamma = 5/3$ is either of Type SF or FSF, for any accretor size and any Mach number at infinity*.

3.3.2. Consequence for nearly isothermal supersonic flows

The Hoyle-Lyttleton limit for the mass accretion rate at high Mach numbers requires that the accreted matter comes from a cylinder with a radius scaling like the accretion radius (Hoyle & Lyttleton 1939). If γ is close to unity, the sonic spherical radius r_0 is $\mathcal{M}_\infty^2/4$ larger than the accretion radius $r_{\rm A}$:

$$\frac{r_0}{r_{\rm A}} = \frac{5-3\gamma}{8}\frac{\mathcal{M}_\infty^2}{1+\frac{\gamma-1}{2}\mathcal{M}_\infty^2} ,$$

$$\sim \frac{\mathcal{M}_\infty^2}{4} \text{ for } \gamma = 1 . \quad (34)$$

If such a flow were of Type F, the geometrical property $\mathcal{P}$ would imply that the sonic surface goes out as far as $\mathcal{M}_\infty^2/4$ times the accretion radius. This leaves only two possibilities for a stationary flow:

(i) the accretor is able to keep material bound up to distances comparable to $r_0 \gg r_{\rm A}$, and the mass accretion rate is infinitely larger than the Hoyle-Lyttleton limit. This is the case of the spherical flows we shall study in Sect. 5.

(ii) the accretor cannot retain material at such large distances, and the flow is of Type SF or FSF, as observed in numerical simulations with γ close to one by Ishii et al. (1993) and Ruffert (1996).
Let us note that the artificially constructed Type F geometry, where the distance of the stagnation point exceeds r_0, while the accreted matter collects within a cylinder of radius $\sim r_{\rm A}$, would be strongly unstable to the Kelvin-Helmholtz instability: the growth rate would scale like $\sim c_\infty/r_{\rm A}$ while the time needed to reach the accretor would scale like $\sim c_\infty/r_0$.

Fig. 4. Comparison of the accretion radius $r_{\rm A}$ with the sonic radius r_0 depending on the values of γ and $\mathcal{M}_\infty$. The thin solid line indicates the region of parameters where the kinetic energy is equal to the thermal energy. The value of $r_{\rm A}/r_0$ is indicated on the dashed and dotted curves

Consequently, we rule out the possibility that the sonic surface is detached in the case of an isothermal stationary flow. According to Eq. (34), the spherical sonic radius is larger than the accretion radius at high Mach numbers if (see also Fig. 4)

$$1 \le \gamma < \frac{9}{7} . \quad (35)$$

4. Asymptotic expansions near the accretor

Spherically symmetric accretion flows with $1 < \gamma < 5/3$ are separated into two distinct classes, depending on whether the flow is subsonic or supersonic at the accretor boundary (Bondi 1952). We learnt from Eq. (26) in Sect. 2.3 that these two branches of solutions also exist for axisymmetric flows, for a given value of the local mass flux at the surface of the accretor. The azimuthal parameter θ, however, introduces an additional degree of freedom, such that the solution might be subsonic in an angular sector, and supersonic in an other (i.e. for a sonic surface attached to the accretor). We must also distinguish between angular directions towards which the flow lines converge (direction of "accreting" flow lines), and directions along which no gas is accreted (direction of "passing" flow lines). By conducting a local analysis, we aim to clarify the various possible configurations.

4.1. Definition of regular and singular accretion

For each flow line (indexed by ϖ) reaching the accretor, we denote by $\theta_0(\varpi)$ the angle between the velocity vector $\boldsymbol{v}$ and the axis of symmetry, when $r \to 0$. Our notations are illustrated in Fig. 5. We define the direction $\theta = 0$ along the axis of symmetry on the downstream side of the accretor, so that the function $\theta_0(\varpi)$ decreases monotonically in the interval $[0, \varpi_0]$, with $\theta_0(0) = \pi$ and $\theta_0(\varpi_0) = 0$. We define θ_c as the largest azimuthal angle, at $r \to 0$, among all the converging flow lines, apart from the axis of symmetry:

$$\theta_c \equiv \mathrm{Max}\{\theta_0(]0, \varpi_0[)\} . \tag{36}$$

This angle can be smaller than π. In particular, $\theta_c < \theta_{sh}$ for flows of Type FSF. Without loosing any significant physical generality, we can assume that $]0, \theta_c[\subset \{\theta_0(]0, \varpi_0[)\}$ in the BHL flow.

Fig. 5. Illustration of our notations $\theta_c, \varpi, \theta_0(\varpi)$

Near the surface of the accretor, let us denote by $2\pi \dot{m}_0(\theta) \sin\theta \mathrm{d}\theta$ the local flux of mass between the azimuthal angles θ and $\theta + \mathrm{d}\theta$:

$$\dot{m}_0(\theta) \equiv \lim_{r\to 0} -r^2 \rho v_r , \tag{37}$$

$$= \lim_{r\to 0} - \left[\frac{(2GM)^{\frac{\gamma+1}{2}}}{\gamma}\right]^{\frac{1}{\gamma-1}} \frac{\mathrm{e}^{-S}}{\sin\theta} \frac{\partial \Psi}{\partial \theta} , \tag{38}$$

$$= \lim_{r\to 0} \frac{\mathrm{e}^{-S} \mathcal{M} \cos\beta}{\gamma^{\frac{1}{\gamma-1}} r^{\frac{5-3\gamma}{2(\gamma-1)}}} \left[\frac{2GM(1+\bar{r})}{\mathcal{M}^2 + \frac{2}{\gamma-1}}\right]^{\frac{\gamma+1}{2(\gamma-1)}} . \tag{39}$$

Since the stream function is bounded in the flow (Eq. 24), integrating Eq. (23) with respect to r implies:

$$\lim_{r_\star \to 0} \beta \frac{\partial \Psi}{\partial \theta} = 0 \quad \text{for } \theta \in [0, \pi] . \tag{40}$$

Thus, if the mass accretion rate $\dot{m}_0$ is locally not zero, the flow lines become locally radial when $r \to 0$ (no "spiraling" of the flow lines). On the other hand, if the flow lines are not radial, Eq. (38) implies that the mass accretion rate is zero in this direction (passing flow lines).

Note that along a direction of accretion, we can consider a flux tube of cross section Φ_ϖ around the flow line such that $\theta_0(\varpi) = \theta$, and write Eq. (37) as follows:

$$\dot{m}_0(\theta_0(\varpi)) = -(\rho v \Phi_\varpi) \lim_{r\to 0} \frac{r^2}{\Phi_\varpi} . \tag{41}$$

The quantity $\dot{m}_0$ is consequently finite only if the flow tubes are asymptotically conical ($\Phi_\varpi(r) \sim r^2$). This leads us to call *regular* the accretion onto a point–like accretor such that $\dot{m}_0$ remains finite, and *singular* when it is locally infinite.

We can also express the local mass accretion rate in terms of the mass flux between the cylinders of radii ϖ and $\varpi + \mathrm{d}\varpi$ at infinity:

$$\dot{m}_0(\theta_0(\varpi)) = -\frac{\rho_\infty v_\infty}{\frac{\sin\theta_0}{\varpi} \frac{\mathrm{d}\theta_0}{\mathrm{d}\varpi}} . \tag{42}$$

Thus singular accretion corresponds to a localized azimuthal angle θ_0 where $\mathrm{d}\theta_0/\mathrm{d}\varpi = 0$. An example of singular accretion is the self-similar solution found by Bisnovatyi-Kogan et al. (1979), where the whole accretion is along a single azimuthal angle $\theta_k = \theta_0(]0, \varpi_0])$.

For a regular flow ($\Phi_\varpi(r) \sim r^2$), we take the limit of Eq. (31) when $r \to 0$ and obtain, along a given flow line,

$$\frac{\partial \log \mathcal{M}^2}{\partial \log r} \sim \frac{5 - 3\gamma}{2(\gamma - 1)} \frac{2 + (\gamma - 1)\mathcal{M}^2}{1 - \mathcal{M}^2} . \tag{43}$$

This equation shows that for $\gamma < 5/3$, the Mach number along regular flow lines either tends to zero or to infinity when approaching the accretor. As in the case of spherical accretion (Bondi 1952) no intermediate finite Mach number is possible. Moreover, this equation proves, by continuity, that a mixed subsonic/supersonic accretion requires a singular accretion at the transition if $\gamma < 5/3$. The sonic surface may still reach the accretor in a regular flow, by separating a region of supersonic accretion from a subsonic region of passing flow lines, as we shall see in Sect. 4.5.

We will now examine the different regions of passing flow lines, supersonic and subsonic regular accretion successively, for $\gamma < 5/3$, and treat the case $\gamma = 5/3$ separately. We shall use the generic name $\epsilon(r)$ for a function which tends to zero with r, and the subscript 0 for the limit of functions when $r \to 0$.

4.2. Region of passing flow lines $\theta \in]\theta_c, \pi[$ for $\gamma \le 5/3$

Since the flux of mass is zero, $\beta_0(\theta)$ cannot vanish in the interval $]\theta_c, \pi[$. According to our sign convention in Sect. 4.3.3 and the definition of β in Eq. (11),

$$\beta_0(\theta) > 0 \quad \text{for } \theta \in]\theta_c, \pi[\ . \tag{44}$$

Since $\beta_0(\pi) = \beta(\theta_c) = 0$, the function β_0 must have a maximum in the interval $]\theta_c, \pi[$.

(i) If the shock is detached, the entropy is finite in the flow. According to Eq. (39), the Mach number must either diverge or tend to zero in order to satisfy $\dot{m}_0 = 0$.
Let us suppose that $\mathcal{M} \to \infty$. We use Eq. (16) and obtain:

$$w = -\frac{v}{2r}\sin\beta_0\left(1 + 2\frac{\partial\beta_0}{\partial\theta}\right)(1 + \epsilon(r)) \ . \tag{45}$$

Using the vorticity equation (10), the entropy gradient can be expressed as:

$$\nabla S = \frac{\gamma\mathcal{M}^2}{2r}\sin\beta_0\left(1 + 2\frac{\partial\beta_0}{\partial\theta}\right)(1 + \epsilon(r)) \ . \tag{46}$$

Integrating this equation over a segment between $\theta = \pi$ and $\theta = \theta_{\max}$, for $r \to 0$, contradicts the fact that the entropy is bounded for a flow with a detached shock. Consequently the Mach number tends to 0 when $r \to 0$, and $\theta_{so} \le \theta_c$. *We conclude that all the flows with a detached shock and $\theta_c < \pi$ are of Type SF.*

(ii) If the shock is attached, the incoming supersonic velocity diverges near the accretor like $r^{-1/2}$ when $r \to 0$. We decompose it into a parallel and a perpendicular component with respect to the shock. The Mach number $\mathcal{M}_{2\perp}$ associated to the component of the velocity, after and perpendicular to the shock, is subsonic according to the Rankine–Hugoniot jump conditions (see e.g. Landau & Lifschitz 1987):

$$\lim_{r\to 0}\mathcal{M}_{2\perp}(\theta_{sh}) = \frac{\gamma - 1}{2\gamma} \ . \tag{47}$$

The Mach number $\mathcal{M}_{2\parallel}$ associated to the component parallel to the shock can be supersonic, but not arbitrarily large:

$$\lim_{r\to 0}\mathcal{M}_{2\parallel}(\theta_{sh}) = \frac{\gamma + 1}{[2\gamma(\gamma - 1)]^{\frac{1}{2}}}\frac{1}{\tan\beta(\theta_{sh})} \ . \tag{48}$$

The total Mach number immediately after the attached shock is consequently finite when $r \to 0$. This result will be important in order to study the local stability of such flows to the Rayleigh–Taylor instability.

4.3. Region of regular supersonic accretion for $\gamma < 5/3$

If $\mathcal{M} \to \infty$ and $\dot{m}_0$ is finite, Eqs. (16)–(19) can be expanded as follows:

$$v_r = -\left(\frac{2GM}{r}\right)^{\frac{1}{2}}(1 + \epsilon(r)) \ , \tag{49}$$

$$\rho = \dot{m}_0\left(\frac{1}{2GMr^3}\right)^{\frac{1}{2}}(1 + \epsilon(r)) \ , \tag{50}$$

$$c = \left(\mathrm{e}^{S_0}\dot{m}_0\right)^{\frac{\gamma-1}{2}}\frac{\gamma^{\frac{1}{2}}}{(2GMr^3)^{\frac{\gamma-1}{4}}}(1 + \epsilon(r)) \ , \tag{51}$$

$$P = \mathrm{e}^{(\gamma-1)S_0}\dot{m}_0^{\gamma}\left(\frac{1}{2GMr^3}\right)^{\frac{\gamma}{2}}(1 + \epsilon(r)) \ , \tag{52}$$

$$\mathcal{M} = \left(\frac{\mathrm{e}^{-S_0}}{\dot{m}_0}\right)^{\frac{\gamma-1}{2}}\frac{(2GM)^{\frac{\gamma+1}{4}}}{\gamma^{\frac{1}{2}}r^{\frac{5-3\gamma}{4}}}(1 + \epsilon(r)) \to \infty \text{ when } r \to 0 \ . \tag{53}$$

The first order azimuthal velocity can be estimated using Eq. (40) in the azimuthal Euler Eq. (20). If the pressure is not spherically symmetric to first order,

$$\frac{1}{\rho}\frac{\partial P}{\partial\theta} = -\frac{3}{2}(2 - \gamma)v_r v_\theta(1 + \epsilon(r)) \ , \tag{54}$$

$$v_\theta = \mathcal{O}\left(r^{\frac{4-3\gamma}{2}}\right) \ . \tag{55}$$

v_r being negative, the azimuthal velocity is oriented towards the region of increasing pressure. The azimuthal pressure force is balanced by this dynamical term. We deduce from Eqs. (11) and (55) an upper bound for the departure from spherical symmetry of the function β:

$$\lim_{r\to 0}\left(\frac{\partial\log\beta}{\partial\log r}\right) \ge \frac{5 - 3\gamma}{2} \ . \tag{56}$$

By studying the leading terms of Eq. (27) when $r \to 0$, we derive in Appendix C a lower bound for the departure from spherical symmetry of the function β, if the entropy of the flow is not uniform:

$$\lim_{r\to 0}\left(\frac{\partial\log\beta}{\partial\log r}\right) \le 5 - 3\gamma \quad \text{if } S'(\Psi) \ne 0 \ . \tag{57}$$

On the other hand, the function β may approach 0 much more rapidly than $\sim r^{5-3\gamma}$ if the entropy is uniform. To phrase it more qualitatively, the presence of an entropy gradient sets a lower bound on the "bending" of the flow lines near the accretor. If a parallel can be drawn with the simpler case of two-dimensional supersonic flow past a concave profile (e.g. Landau & Lifshitz 1987), this "bending" could be related to the formation of long–lived radial shocks in the supersonic region of flows with a non–uniform entropy, as observed in numerical simulations with $\gamma = 4/3$ in 2–D (Hunt 1979) and 3–D (Ruffert 1995).

Because the radial velocity (49) is spherically symmetric to first order, the azimuthal dependence of the accreted momentum ρv comes mainly from the azimuthal dependence of the density ρ, which we decompose into the contributions of pressure and entropy,

$$\rho(r,\theta) = P^{\frac{1}{\gamma}}(r,\theta)\exp\left(-\frac{\gamma - 1}{\gamma}S(r,\theta)\right) \ . \tag{58}$$

Thus we expect that for a flow with uniform entropy (no shock), the mass is mainly accreted from the hemisphere where the pressure is the highest. The geometrical interpretation of Eq. (32) implies that near the axis of symmetry (i.e. for $\theta \sim 0$ and $\theta \sim \pi$), the azimuthal speed is oriented away from the axis where $r_{\rm so} > r_0$, and towards the axis where $r_{\rm so} < r_0$. If one assumes that the sign of the azimuthal velocity does not change in the supersonic region between the sonic surface and the accretor, Eq. (54) indicates that the highest pressure is on the side of the accretor where $r_{\rm so} > r_0$.

For an isentropic subsonic flow, the natural orientation of the azimuthal velocity is set by the sign of the angular momentum of the fluid element at infinity. A subsonic medium would flow from the *left* of the accretor in Fig. 3. Therefore the sonic surface is displaced opposite to the direction of the flow at infinity, and the maximum flux of mass is expected on the back hemisphere of the accretor. Indeed, in the subsonic numerical simulations of a flow with $\gamma = 4/3$ by Hunt (1979) in 2–D, and by Ruffert (1995) in 3–D, the sign of the accreted linear momentum is negative for the smallest accretor considered.

If the flow is supersonic at infinity, the position of the shock along the axis is displaced in the direction of the flow, compared to its position for a spherical flow with same kinetic and thermal energies at infinity, because there is now a leakage of gas away from the accretor and the pressure ahead of the accretor is lower than in the corresponding spherical case. The sonic point along the axis is displaced accordingly. The sonic surface is consequently shifted in the direction of the flow, leading to a highest pressure on the front hemisphere of the accretor. The simplest configuration is the one in Fig. 3, where the supersonic flow now comes from the *right* of the accretor.

Nevertheless, the entropy generated by the shock decreases with increasing distance from the axis of symmetry (see Appendix F), so that entropy and pressure contribute in opposite directions to the density in Eq. (58), precluding a direct conclusion about its azimuthal distribution near the accretor. However, the accreted linear momentum is negative in the numerical simulations by Ruffert (1996 and references therein) indicating that the entropy effect is stronger than the pressure effect.

4.4. Region of regular subsonic accretion for $\gamma < 5/3$

If $\mathcal{M} \to 0$ and $\dot m_0$ is finite, Eqs. (16)–(19) can be written as follows:

$$v_r = e^{S_0}\dot m_0 \left[\frac{\gamma}{(\gamma-1)GM}\right]^{\frac{1}{\gamma-1}} r^{\frac{3-2\gamma}{\gamma-1}}(1+\epsilon(r)) \ , \tag{59}$$

$$\rho = e^{-S_0}\left[\frac{(\gamma-1)GM}{\gamma r}\right]^{\frac{1}{\gamma-1}} (1+\epsilon(r)) \ , \tag{60}$$

$$c = \left[\frac{(\gamma-1)GM}{r}\right]^{\frac{1}{2}} (1+\epsilon(r)) \ , \tag{61}$$

$$P = e^{-S_0}\left[\frac{(\gamma-1)GM}{\gamma r}\right]^{\frac{\gamma}{\gamma-1}} (1+\epsilon(r)) \ , \tag{62}$$

$$\begin{aligned}\mathcal{M} &= \frac{\gamma^{\frac{1}{\gamma-1}} e^{S_0}\dot m_0}{[(\gamma-1)GM]^{\frac{\gamma+1}{\gamma-1}}} r^{\frac{5-3\gamma}{2(\gamma-1)}}(1+\epsilon(r)) \\ &\to 0 \text{ when } r \to 0 \ .\end{aligned} \tag{63}$$

We use Eqs. (59) and (40) to estimate the dynamical terms balancing the azimuthal pressure force in Eq. (20) and obtain:

$$\frac{1}{\rho}\frac{\partial P}{\partial \theta} \ll \mathcal{O}\left(r^{\frac{2(3-2\gamma)}{\gamma-1}}\right) \ll \mathcal{O}\left(r^{-1}\right) \ . \tag{64}$$

Comparing this to the first order of $P/\rho \sim c^2$ given by Eq. (61), we conclude for $\gamma < 5/3$ that *the pressure in the regular subsonic region is spherically symmetric to first order when* $r \to 0$. Thus Eq. (62) implies that the subsonic flow for $\gamma < 5/3$, with its first order expansions (59)–(63), is possible *only if the entropy is uniform*.

In particular, the spherical solution proposed by Theuns & David (1992), connecting a supersonic solution to a subsonic solution through a shock, cannot resist the slightest asphericity if the accretor is point–like. The azimuthal pressure force due to the convergence of flow lines of different entropies is too big to be balanced by dynamical forces in the regular subsonic region close to the accretor. Nevertheless, this constraint of the azimuthal Euler equation is less stringent for large accretor sizes. One can also argue that the radiative processes near the surface of the star may homogenize the entropy, and allow for a spherically symmetric subsonic accretion.

The entropy in flows of Types SF and FSF is a *strictly* decreasing quantity along the shock:

(i) In Type FSF flows, the velocity diverges to infinity when $r_{\rm sh} \to 0$, thus the entropy created along the shock decreases strictly with distance from the accretor for Type FSF flows, precluding a subsonic accretion with a uniform entropy.

(ii) For Type SF flows, we show in Appendix F that the entropy created along the shock strictly decreases with distance from the axis of symmetry.

We conclude that there cannot be a region of regular subsonic accretion in shocked flows with $\gamma < 5/3$, for a point–like accretor. The subsonic region may reach the surface of the accretor for any finite size, but *the mass accreted in the shocked regular subsonic region* $\theta > \theta_{\rm so}$ *tends to zero when the accretor size decreases to zero*.

4.5. The sonic surface for Type SF and FSF shocked flows $\gamma < 5/3$

Since no regular subsonic accretion is possible with a non–uniform entropy, all the regular flow lines are ultimately supersonic when they reach the point–like accretor ($\theta_{\rm c} \le \theta_{\rm so}$). Note that in the singular solutions by Bisnovatyi-Kogan et al. (1979), the Mach number tends to infinity along each flow line.

Together with the results of Sect. 4.2, we conclude that for a flow with a detached shock, and $\gamma < 5/3$,

$$\theta_{\rm c} = \theta_{\rm so} \ . \tag{65}$$

According to Eq. (32), the cross section of the flow tube reaching the sound speed at the surface of the accretor varies like:

$$\frac{\partial \log \Phi}{\partial l} \frac{\partial l}{\partial \log r} = \frac{\gamma + 1}{2(\gamma - 1)} > 2 \ . \tag{66}$$

Comparing this equation to Eq. (41), we conclude that the azimuthal angle $\theta_{\rm so}$ cannot be a direction of regular accretion. However, $\theta_{\rm so}$ is not necessarily a direction of singular accretion. A regular flow simply requires that $\theta_{\rm c} \notin \{\theta_0(]0, \varpi_0[)\}$.

4.6. The particular case $\gamma = 5/3$

We denote by $\mathcal{M}_0(\theta)$ the limit of the Mach number along a converging flow line. For $\theta \in]0, \theta_{\rm c}[$, Eq. (39) implies that the local mass accretion rate $\dot{m}_0$ is always finite, its maximum value being reached for $\mathcal{M}_0 = 1$:

$$\begin{aligned} \dot{m}_0 \ &= \ \left(\frac{3}{5}\right)^{\frac{3}{2}} 4G^2M^2 {\rm e}^{-S_0} \frac{\mathcal{M}_0}{\left(\mathcal{M}_0^2 + 3\right)^2} \ , & (67) \\ &\leq \ \left(\frac{3}{5}\right)^{\frac{3}{2}} \frac{G^2M^2}{4} {\rm e}^{-S_0} \ . & (68) \end{aligned}$$

The pressure forces for $\gamma = 5/3$ are strong enough to impede an arbitrarily high mass flux, even locally. Thus accretion flows with $\gamma = 5/3$ are always regular, and the maximum mass accretion rate is the spherical Bondi value. This result is particularly important to understand the instability observed in numerical simulations. Since the most unstable simulations were observed with $\gamma = 5/3$, we can restrict our future stability analysis to the simpler case of regular flows.

Using Eq. (16) and (40) in the azimuthal Euler Eq. (20), we find that the azimuthal pressure force is bounded by Eq. (64). Comparing it to Eqs. (17) and (19), we conclude that the pressure is spherically symmetric to first order for $\theta \in]0, \theta_{\rm c}[$. According to Eq. (58), the density is spherically symmetric to first order if there is no shock (uniform entropy), but increases towards the back hemisphere if there is a shock.

With Eqs. (16) to (19), we conclude that:

(i) in the absence of a shock, the pressure, density, temperature, velocity and Mach number are spherically symmetric to first order when $r \to 0$. The accreted momentum is therefore spherically symmetric as well. This is confirmed by the numerical simulations by Ruffert (1994b), with $\mathcal{M}_\infty = 0.6$ and $\gamma = 5/3$. The accreted linear momentum decreases to zero with the size of the accretor (see Fig. 2, model "SL", "SM", "SS"). Moreover, the uniform Mach number $\mathcal{M}_0$ must be lower than or equal to one because of the property $\mathcal{P}$.

(ii) if a shock is present, the pressure is spherically symmetric to first order when $r \to 0$, the temperature and entropy increase towards the upstream hemisphere, and the density, the velocity and the Mach number increase towards the downstream hemisphere. Consequently, more mass is accreted from the downstream hemisphere than from the upstream hemisphere. This is also confirmed by the numerical simulations with $\gamma = 5/3$ by Ruffert (1994b), at $\mathcal{M}_\infty = 1.4$. This trend persists in the unstable cases, simulated by Ruffert & Arnett (1994) at $\mathcal{M}_\infty = 3$, and Ruffert (1994b), at $\mathcal{M}_\infty = 10$.

Thus we disagree with Hunt (1971), who chose the Mach number at the surface of the accretor $\mathcal{M}_0$ in order to maximize the mass accretion rate. As can be checked from Eq. (67), the highest mass accretion rate is obtained for $\mathcal{M}_0 = 1$. The Mach number at the surface of the accretor is, however, not a free parameter, but is constrained by the distribution of entropy. Let S_1 be the entropy of the flow line reaching the accretor with $\mathcal{M}_0 = 1$. The pressure being uniform, Eq. (19) implies that the final Mach number of the flow line indexed by ϖ depends on its entropy $S(\varpi)$ according to:

$$\mathcal{M}_0^2(\varpi) = 4{\rm e}^{\frac{2}{5}(S_1 - S(\varpi))} - 3 \ . \tag{69}$$

The erroneous conclusion of Hunt (1971), that the axisymmetric flow with $\gamma = 5/3$ never becomes supersonic close to the accretor is in contradiction with the 3–D numerical simulations (see Fig. 17 in Ruffert 1994b). It is even in contradiction with the Mach number $\mathcal{M}_0(\theta = \pi) \sim 2.1$ that one can deduce from the velocity, entropy and density displayed in Figs. 5, 6 and 8 in Hunt (1971) for $\mathcal{M}_\infty = 2.4$.

In a similar way as Eq. (C10), obtained for $\gamma < 5/3$, Eq. (69) shows that the functions $S, \beta, \mathcal{M}$ also cease to be independent at the boundary of the accretor for $\gamma = 5/3$ if $r_\star \to 0$. For a given distribution of entropy $S(\Psi)$, the only degree of freedom left by Eqs. (38), (67) and (69) is the value of S_1, i.e. the amount of mass accreted subsonically. The value of $S_{\rm 1opt}$ which maximizes the total mass accretion rate satisfies an integral equation depending only on $S(\Psi)$, which can be solved numerically. Thus if the shape of the shock is known, the distribution $S(\Psi)$ is fixed by the Rankine-Hugoniot jump conditions along the shock (see Appendix F), and the total mass accretion rate $\dot{M}\{S(\Psi), S_1\}$ is bounded by this maximum value $\dot{M}\{S(\Psi), S_{\rm 1opt}\}$.

Since the subsonic accretion of material with a non–uniform entropy is possible for $\gamma = 5/3$, we only have the inequality $\theta_{\rm so} \geq \theta_{\rm c}$. Nevertheless, the difference of entropies in the region of subsonic accretion is limited by the Eq. (69) to:

$$S_1 - S(\varpi = 0) \leq \frac{5}{2} \log \frac{3}{4} \sim 0.72 \ . \tag{70}$$

An angular sector of passing flow lines may exist, and is described in Sect. 4.2.

An estimate of the first order departures from spherical symmetry is obtained by writing the differential Eq. (27) to first order in the vicinity of $r = 0$ (see Appendix D). This provides us with a lower bound on the departure from sphericity for the function β, when the entropy is not uniform:

$$0 \leq \lim_{r \to 0} \left(\frac{\partial \log \beta}{\partial \log r}\right) \leq 1 \ \ \text{if} \ \ S'(\Psi) \neq 0 \ . \tag{71}$$

As in Sect. 4.3, this "bending" of the flow lines enforced by the entropy gradient could be related to the formation of long–lived radial shocks in the supersonic region of flows with a non–uniform entropy, as observed in numerical simulations (Ruffert 1994b).

5. Mass accretion rate for a spherically symmetric flow with non–vanishing kinetic and thermal energies at infinity

5.1. Analytical estimates of the mass accretion rate

Only two situations are known to have analytical solutions:

(i) Spherically symmetric accretion from a gas at rest at infinity (Bondi 1952). The mass accretion rate of the unique transsonic solution is:

$$\dot{M}_{\rm B} \equiv \frac{4\pi G^2 M^2 \rho_\infty}{c_\infty^3} \left[\frac{1}{2}\right]^{\frac{\gamma+1}{2(\gamma-1)}} \left[\frac{4}{5-3\gamma}\right]^{\frac{5-3\gamma}{2(\gamma-1)}} , \tag{72}$$

(ii) Axisymmetric accretion from a gas with negligible temperature (Hoyle and Lyttleton 1939):

$$\dot{M}_{\rm HL} \equiv \frac{4\pi G^2 M^2 \rho_\infty}{v_\infty^3} . \tag{73}$$

Other normalizations were also proposed to account for the pressure effects with more realism, e.g. a factor 2 lower (Bondi & Hoyle 1944).

In order to bridge the analytical gap between the case of spherical accretion described by $\dot{M}_{\rm B}$ (Eq. 72) and the case of supersonic accretion from a gas of negligible temperature described by $\dot{M}_{\rm HL}$ (Eq. 73), Bondi (1952) proposed a simple interpolation formula, meant to give the correct order of magnitude. Here we use the normalization adopted later by Shima et al. (1985) and Ruffert & Arnett (1994) on the basis of numerical simulations, which is a factor 2 larger:

$$\dot{M}_{\rm BH} \equiv \frac{4\pi G^2 M^2 \rho_\infty}{(c_\infty^2 + v_\infty^2)^{\frac{3}{2}}} . \tag{74}$$

It has the advantage of being very simple and giving a roughly correct limiting behaviour for $v_\infty \to 0$ or $v_\infty \to \infty$. However, because it is independent of γ, it is bound to fail to reproduce quantitatively the analytical spherical accretion rate $\dot{M}_{\rm B}$, which varies by a factor ~ 3 between $\gamma = 5/3$ and $\gamma = 4/3$. Moreover, numerical simulations have shown typical discrepancies of a factor 2–3 with this formula for various Mach numbers (see Fig. 9 and Fig. 10, and also Hunt 1979).

5.2. The mass accretion rate of a shocked spherical flow

An intermediate situation, also analytically tractable, is the case of a spherical accretion with a constant kinetic energy at infinity: the gas is "thrown" towards the accretor, from a reservoir at infinity where the flow speed is v_∞, the density ρ_∞ and the sound speed c_∞ are uniform and non–vanishing, i.e. the kinetic energy and the thermal energies are constant at infinity.

To this end, we imagine converging radial "pipes" of constant cross section (Fig. 6). They remain separate up to a minimum radius $r_{\rm p}$ at which they merge. For a given distance $r_{\rm p}$, if a stationary solution exists, the mass accretion rate imposed at infinity would be:

$$\dot{M} = 4\pi r_{\rm p}^2 \rho_\infty v_\infty . \tag{75}$$

Fig. 6. The gas is "thrown" towards the accretor in a spherically symmetric way. "Pipes" of constant cross section are used to allow for both a constant thermal and kinetic energy at infinity. The accretion radius $r_{\rm A}$ (full circle) can be smaller than the sonic radius r_0 (dotted circle). A spherical shock is represented by the thick dotted circle.

Thus $2r_{\rm p}$ is also the radius of a cylinder containing the accreted material in an axisymmetric flow where the transition between the parallel flow at infinity and the spherical flow near the accretor (and also the decrease of angular momentum along each flow line) would be artificially driven through such pipes. This situation allows us to understand how the kinetic energy influences the mass accretion rate, for a gas with an adiabatic index γ.

For spherical flows, the mass accretion rate of the stationary solution is determined by the regularity condition at the sonic radius. We obtain exactly the same dimensionless quartic equation as in the classic spherical Bondi accretion, determining, in the notations of Theuns & David (1992), $\tilde{r}$ as a function of $\tilde{c}^2$ (see for example their Eq. 2.9), except that the velocities v, c and distance r are now normalized differently:

$$v = \tilde{v} c_\infty \left(1 + \frac{\gamma-1}{2}\mathcal{M}_\infty^2\right)^{1/2} , \tag{76}$$

$$r = \tilde{r} \frac{GM}{c_\infty^2 + \frac{\gamma-1}{2} v_\infty^2} . \tag{77}$$

For spherically symmetric flows, the regularity condition at the sonic radius fixes the mass accretion rate $\dot{M}_{\rm sph}$ for the unique transsonic solution: by integrating the mass flux (29) over the sonic sphere ($\mathcal{M}(r_0) = 1$), we obtain:

$$\dot{M}_{\rm sph} = 4\pi G^2 M^2 \left[\frac{1}{2}\right]^{\frac{\gamma+1}{2(\gamma-1)}} \left[\frac{4(\gamma-1)}{5-3\gamma}\right]^{\frac{5-3\gamma}{2(\gamma-1)}} \frac{\rho_\infty}{c_\infty^{\frac{2}{\gamma-1}}} {\rm e}^{-\Delta S} B_\infty^{\frac{5-3\gamma}{2(\gamma-1)}} , \tag{78}$$

where ΔS is the entropy gained when passing through a spherical shock, if the flow at infinity is supersonic.

Introducing the entropy S_∞ of the gas at infinity defined by Eq. (3), the spherical mass accretion rate can also be written:

$$\dot{M}_{\rm sph} = 4\pi G^2 M^2 \left[\frac{1}{2}\right]^{\frac{\gamma+1}{2(\gamma-1)}} \left[\frac{4(\gamma-1)}{5-3\gamma}\right]^{\frac{5-3\gamma}{2(\gamma-1)}} \frac{1}{\gamma^{\frac{1}{\gamma-1}}} {\rm e}^{-(S_\infty+\Delta S)} B_\infty^{\frac{5-3\gamma}{2(\gamma-1)}} . \tag{79}$$

The mass accretion rate is clearly an increasing function of energy B_∞, and a decreasing function of the total entropy $(S_\infty + \Delta S)$.
We now consider the two possible cases of flows with and without a shock separately.

5.2.1. Flows without a shock

According to Eq. (78) when $\Delta S = 0$, we expect the mass accretion rate of isentropic flows to increase with the Mach number:

$$\dot{M}_{\rm sph}(\Delta S = 0) \;=\; \dot{M}_{\rm B}\left[1 + \frac{\gamma - 1}{2}\mathcal{M}_\infty^2\right]^{\frac{5-3\gamma}{2(\gamma-1)}} \;. \qquad (80)$$

This increase of the mass accretion rate with the Mach number for spherical subsonic flows, is not obvious *a priori*. An increase of the speed at infinity acts as an additional external pressure on the flow: according to Eq. (33), the sonic radius r_0 decreases, and Eq. (29) shows that the momentum increases. However, the decrease of the area of the sonic surface, over which the momentum must be integrated to obtain the mass accretion rate, is more than compensated by the increase of momentum, for $\gamma < 5/3$. The mass accretion rate is independent of the Mach number for $\gamma = 5/3$.

5.2.2. Flows with a shock

Increasing the velocity of the flow at infinity increases its total energy B_∞, but passing through a shock also increases its entropy. According to Eq. (79), these two effects act in opposite directions on the mass accretion rate. Whether the mass accretion is eventually increased or decreased depends on the position of the shock, which can be determined numerically as follows: for high Mach numbers, we choose the distance of the pipes, so that the sound velocity prior to the shock c_1 equals the sound velocity at infinity $c_1 = c_\infty$. This corresponds to the position $r_{\rm p} > r_{\rm sh}$ such that the dilution due to gravitational acceleration is balanced by the concentration of flow lines. We make this particular choice by analogy with the case of axisymmetric accretion with a detached bow shock: we show in Appendix E that the density enhancement, along the axis of symmetry, before the shock, is smaller than a factor 2 if $r_{\rm sh} > 0.03 r_{\rm A}$.
For each radius r, the Bernoulli equation (7) determines the supersonic speed $v_1(r)$ and Mach number $\mathcal{M}_1(r)$ prior to the shock. Using the Rankine–Hugoniot jump conditions, we can compute the entropy jump $\Delta S(r)$ and the corresponding subsonic velocity $v_2(r)$ after the shock, if the shock occurs at that radius r:

$$v_1(r) \;=\; \left(v_\infty^2 + \frac{2GM}{r}\right)^{1/2} = \mathcal{M}_1(r) c_\infty \;, \qquad (81)$$

$$v_2(r) \;=\; \frac{2 + (\gamma - 1)\mathcal{M}_1^2}{(\gamma + 1)\mathcal{M}_1^2} v_1(r) \;, \qquad (82)$$

$$e^{-\Delta S(r)} \;=\; \left[\frac{(\gamma + 1)\mathcal{M}_1^2}{2 + (\gamma - 1)\mathcal{M}_1^2}\right]^{\frac{\gamma}{\gamma-1}} \left[\frac{\gamma + 1}{2\gamma\mathcal{M}_1^2 - \gamma + 1}\right]^{\frac{1}{\gamma-1}} . \qquad (83)$$

For a given entropy ΔS and Bernoulli constant B_∞, we denote the velocity profile of the unique transsonic solution, by $v[\Delta S, B_\infty](r)$. The unique shock position $r_{\rm sh}$ corresponds to the solution of the equation

$$v_2(r_{\rm sh}) = v[\Delta S(r_{\rm sh}), B_\infty](r_{\rm sh}) \;. \qquad (84)$$

Fig. 7. Position of the shock $r_{\rm sh}$, in accretion radii, as a function of $\mathcal{M}_\infty$. The value of γ is indicated on each curve.

The position of the shock determined by this procedure is shown in Fig. 7, as a function of γ and $\mathcal{M}_\infty$. Except for values of γ close to $5/3$, the spherical shock distance is larger than the accretion radius, and thus larger than was observed in numerical simulations of the axisymmetric BHL flow (typically $r_{\rm sh} \sim 0.2 r_{\rm A}$).
The spherical mass accretion rate is given by the Eq. (80) diminished by a factor $\exp(-\Delta S(r_{\rm sh})) < 1$ defined in Eq. (83).
Increasing the kinetic energy of the supersonic flow always decreases ultimately the mass accretion rate below the value $\dot{M}_{\rm B}$ obtained for a gas at rest. Between the two opposite tendencies (entropy and energy), the decrease due to entropy will dominate for large Mach numbers, since the effective Mach number $\mathcal{M}_1$ at the shock radius is larger than the Mach number at infinity. For $\mathcal{M}_\infty \gg 1$, Eqs. (79) and (83) imply:

$$\dot{M}_{\rm sph} \sim C(\gamma)\left[\frac{\mathcal{M}_\infty}{\mathcal{M}_1}\right]^{\frac{2}{\gamma-1}} \frac{\rho_\infty}{v_\infty^3} \le C(\gamma)\frac{\rho_\infty}{v_\infty^3} \;. \qquad (85)$$

Moreover, Fig. 7 and Fig. 8 show that the shock radius is proportional to the accretion radius for high Mach numbers, in other words the ratio $\mathcal{M}_\infty/\mathcal{M}_1$ is a non–vanishing constant for high Mach numbers. Apart from a multiplicative factor $C(\gamma)$ depending on γ, the mass accretion rate in this spherical geometry scales like the mass accretion rate $\dot{M}_{\rm HL}$ derived by Hoyle & Lyttleton (1939) for an axisymmetric flow of negligible pressure.

Fig. 8. The mass accretion rate, as a function of $\mathcal{M}_\infty$, in Bondi units $\dot{M}_{\rm B}$ (upper curves) and also in units of the interpolation formula $\dot{M}_{\rm BH}$ (lower curves). The value of γ is indicated on each curve. The mass accretion rate follows the Hoyle–Lyttleton behaviour when the kinetic energy dominates the thermal energy (slope $\mathcal{M}^{-3}$). For a nearly isothermal flow, however, it exceeds the Bondi value if the thermal energy is larger than the kinetic energy. The dotted horizontal line is the mass accretion rate from a gas at rest at infinity.

It is remarkable that the mass accretion rate is asymptotically independent of the value of the sound speed at infinity.

5.3. What is the maximum spherical mass accretion rate ?

We see from Eq. (79) that $\dot{M}_{\rm B}$ is the maximum spherical mass accretion rate for $\gamma = 5/3$. As we shall proceed to show, the situation is very different for γ close to 1. The value of γ defines the strength of a pressure change in response to a density change. Since the pressure gradient is the only force limiting the mass accretion rate, the higher the value of γ, the higher the pressure forces and thus the slower the accretion (see Eq. 72).

An isothermal gas is much more easily "swallowed" by the accretor: a significant increase of the mass accretion rate occurs for $1 < \mathcal{M}_\infty^2 < 2/(\gamma-1)$. In this range, the thermal energy dominates the kinetic energy, and Eq. (33) implies that the sonic radius scales like the Bondi radius $\sim GM/c_\infty^2$. More accurately, taking the Rankine–Hugoniot jump condition (83) in the limit $\gamma \to 1$ and combining with Eq. (79) gives:

$$\dot{M}_{\rm sph}(\gamma \to 1) = \dot{M}_{\rm B}\mathcal{M}_1^2 \exp\left(\frac{\mathcal{M}_\infty^2 - \mathcal{M}_1^2}{2} + \frac{1}{2\mathcal{M}_1^2}\right) . \quad (86)$$

We can estimate the contribution of the exponential factor using the Bernoulli equation (81), for $\gamma \to 1$:

$$0 < \frac{\mathcal{M}_1^2 - \mathcal{M}_\infty^2}{2} = 2\frac{r_0}{r_{\rm sh}} < 2 . \quad (87)$$

Consequently, the mass accretion rate scales like:

$$\dot{M}_{\rm sph}(\gamma \to 1) = \mathcal{O}(\dot{M}_{\rm B}\mathcal{M}_\infty^2) \ \text{ for } \ 1 \ll \mathcal{M}_\infty^2 < \frac{2}{\gamma - 1} . \quad (88)$$

Using the geometrical constraint that $r_{\rm sh} > r_0$, we can also write the mass accretion rate $\dot{M}_{\rm sh}$ as the flux of mass through the shock surface, for $\gamma \to 1$. For high Mach numbers, Eq. (81) ensures that $v_1 \sim v_\infty$, and the density before the shock $\rho_1 \sim \rho_\infty$ because the pipes are of constant cross section. Thus,

$$\dot{M}_{\rm sh} \equiv 4\pi r_{\rm sh}^2 \rho_1 v_1 = \frac{4\pi G^2 M^2 \rho_\infty}{c_\infty^3}\left(\frac{r_{\rm sh}}{r_0}\right)^2 \frac{\mathcal{M}_\infty}{4} . \quad (89)$$

Comparing this equation to Eq. (88), we conclude from $\dot{M}_{\rm sh} = \dot{M}_{\rm sph}$ that the shock radius is a factor $\mathcal{M}_\infty^{1/2}$ larger than the sonic radius. Inserting this result back into Eq. (87), we further conclude that the mass accretion rate is:

$$\dot{M}_{\rm sph}(\gamma \to 1) = {\rm e}^{3/2}\pi \frac{\rho_\infty G^2 M^2}{c_\infty^3}\mathcal{M}_\infty^2 , \quad \text{for } \ 1 \ll \mathcal{M}_\infty^2 < \frac{2}{\gamma - 1} , \quad (90)$$

which is a factor $\mathcal{M}_\infty^2$ larger than the spherical mass accretion rate $\dot{M}_{\rm B}$ from a gas at rest at infinity, and a factor $\mathcal{M}_\infty^5$ higher than the Hoyle–Lyttleton accretion rate $\dot{M}_{\rm HL}$.
We conclude that for values of γ approaching 1, the largest spherical mass accretion rate is:

$$\dot{M}_{\rm max} \sim \frac{2}{\gamma - 1}\dot{M}_{\rm B} , \quad (91)$$

and is reached when the kinetic and thermal energies at infinity are comparable, i.e. :

$$\mathcal{M}_\infty^2 \sim \frac{2}{\gamma - 1} . \quad (92)$$

This scaling obtained in the isothermal limit for high Mach numbers is confirmed by the exact calculation of the mass accretion rate, for any value of γ, through the numerical derivation

of the position of the shock, as shown by Fig. 8.
The entropy–energy approach for a spherical flow has shown us that the mass accretion rate ultimately decreases like the Hoyle–Lyttleton rate when the kinetic energy dominates the thermal energy.
Nevertheless, the mass accretion rate increases considerably above its value at $\mathcal{M}_\infty = 0$, when the kinetic energy is comparable to the thermal energy, i.e. $1 < \mathcal{M}_\infty^2 \sim 2/(\gamma-1)$. This effect is most pronounced for $\gamma \to 1$. Thus the value of the adiabatic index plays a very important role in the determination of the mass accretion rate in the case of spherical accretion with a shock. Similarly, we expect the mass accretion rate of an axisymmetric BHL flow with constant parallel velocities at infinity to depend on the adiabatic index.

6. An interpolation formula for the mass accretion rate of an axisymmetric flow with $\gamma > 9/7$

The axisymmetric mass accretion rate $\dot M_{\rm ax}$ can be formally calculated from the integral of the mass flux along any surface surrounding the accretor. We can decompose the mass accretion into three components,

$$\dot M_{\rm ax} = \dot M_{\rm so} + \dot M_{\rm S} + \dot M_{\rm F} \ , \tag{93}$$

where $\dot M_{\rm so}$ is the mass flux through the sonic surface, $\dot M_{\rm S}$ is the mass flux in the subsonic region (Types SF and FSF), and $\dot M_{\rm F}$ is the mass flux in the supersonic region ahead of the shock (Type FSF only).
The trajectories of the gas in the supersonic region ahead of the accretor are well approximated by hyperbolae, obtained by neglecting the temperature of the gas. $\dot M_{\rm F}$ decreases to zero when the accretor size $r_\star$ decreases to zero (Eddington 1926):

$$\dot M_{\rm F} \sim \pi r_\star (r_{\rm A} + r_\star)\rho_\infty v_\infty \ . \tag{94}$$

According to Sect. 4.4, $\dot M_{\rm S}$ also decreases to zero with decreasing size of the accretor, for shocked flows with $\gamma < 5/3$. Consequently, the mass flux through the sonic surface gives a good estimate of the total mass accretion rate for small accretors:

$$\dot M_{\rm ax} = \dot M_{\rm so}(1+\epsilon(r_\star)) \ \text{ for } \ 1<\gamma<5/3 \ . \tag{95}$$

Using Eq. (29) with $\mathcal{M} = 1$, we can write $\dot M_{\rm so}$ as follows:

$$\dot M_{\rm so} \equiv 4\pi G^2 M^2 \frac{\rho_\infty}{c_\infty^{\frac{2}{\gamma-1}}} \left[\frac{2(\gamma-1)}{\gamma+1}\right]^{\frac{\gamma+1}{2(\gamma-1)}} \int_{\rm sonic} \left[\frac{1+\bar r_{\rm so}}{\bar r_{\rm so}^{\frac{5-3\gamma}{\gamma+1}}}\right]^{\frac{\gamma+1}{2(\gamma-1)}} B_\infty^{\frac{5-3\gamma}{2(\gamma-1)}} {\rm e}^{-\Delta S} \frac{{\rm d}\Phi}{4\pi r_{\rm so}^2} \ . \tag{96}$$

As in the case of spherical accretion, the mass accretion rate is an increasing function of the energy and a decreasing function of the entropy. However, the geometry of the sonic surface also influences the mass accretion rate. We know from Eq. (32) that the shape of the sonic surface $r_{\rm so}(r,\theta)$ is directly related to the shape of the flow lines. In contrast to the energy and the entropy, the geometrical factor depends on the shape of the flow lines at infinity, and is more difficult to estimate since it does not correspond to a conserved quantity. One can try to obtain, for the axisymmetric case, an interpolation formula for the mass accretion rate $\dot M_{\rm I}$, based on the spherical entropy–energy approach.
With some trigonometry we write:

$$\frac{{\rm d}\Phi}{4\pi r_{\rm so}^2} = \left(\cos\beta - \sin\beta \frac{\partial \log r_{\rm so}}{\partial\theta}\right)\frac{\sin\theta}{2}{\rm d}\theta \ . \tag{97}$$

The direction $\theta = 0$ being in the direction of the flow, the axisymmetric sonic surface is described by $r_{\rm so}(\theta)$, with $0 < \theta < \theta_{\rm so}$. For Type F flows, $\theta_{\rm so}$ must be replaced by π in what follows:

$$\dot M_{\rm so} = 4\pi \frac{\rho_\infty G^2 M^2}{c_\infty^3}\left[\frac{1}{2}\right]^{\frac{\gamma+1}{2(\gamma-1)}} \left[\frac{1+\frac{\gamma-1}{2}\mathcal{M}_\infty^2}{\frac{5-3\gamma}{4}}\right]^{\frac{5-3\gamma}{2(\gamma-1)}} \int_0^{\theta_{\rm so}} h(\bar r_{\rm so}){\rm e}^{-\Delta S(\mathcal{M}_1(\theta))}\frac{{\rm d}\Phi}{4\pi r_{\rm so}^2} \ , \tag{98}$$

$$h(\bar r) \equiv \left[\frac{\bar r_0}{\bar r}\right]^{\frac{5-3\gamma}{2(\gamma-1)}} \left[\frac{1+\bar r}{1+\bar r_0}\right]^{\frac{\gamma+1}{2(\gamma-1)}} \ . \tag{99}$$

First note by differentiating $h(\bar r)$ with respect to $\bar r$ that:

$$h(\bar r) \geq h(\bar r_0) = 1 \ , \tag{100}$$

The integral in Eq. (98) can be seen as an average of $h(\bar r_{\rm so})$ times the entropy weighted by the geometrical function ${\rm d}\Phi/4\pi r_{\rm so}^2 > 0$, thus defining an effective entropy corresponding to an effective Mach number $\mathcal{M}_{\rm e} \equiv \mathcal{M}_1(\theta_{\rm e})$:

$$\int_0^{\theta_{\rm so}} h(\bar r_{\rm so}){\rm e}^{-\Delta S(\mathcal{M}_1(\theta))}\frac{{\rm d}\Phi}{4\pi r_{\rm so}^2} \equiv h(\bar r_{\rm so}(\theta_{\rm e})){\rm e}^{-\Delta S(\mathcal{M}_e)}\int_0^{\theta_{\rm so}}\frac{{\rm d}\Phi}{4\pi r_{\rm so}^2} \ . \tag{101}$$

Using Eq. (83) and the definition (72) of $\dot M_{\rm B}$, Eq. (98) becomes:

$$\dot M_{\rm so} = \dot M_{\rm B}\left[1+\frac{\gamma-1}{2}\mathcal{M}_\infty^2\right]^{\frac{5-3\gamma}{2(\gamma-1)}} h(\bar r_{\rm so}(\theta_{\rm e}))\int_0^{\theta_{\rm so}}\frac{{\rm d}\Phi}{4\pi r_{\rm so}^2} \left[\frac{(\gamma+1)\mathcal{M}_{\rm e}^2}{2+(\gamma-1)\mathcal{M}_{\rm e}^2}\right]^{\frac{\gamma}{\gamma-1}} \left[\frac{\gamma+1}{2\gamma\mathcal{M}_{\rm e}^2-\gamma+1}\right]^{\frac{1}{\gamma-1}} \ . \tag{102}$$

One can check that for isentropic flows ($\Delta S = 0$) and small deviations from sphericity ($f(\theta) \sim \beta \sim (\bar r_{\rm so} - \bar r_0) \ll 1$), the mass accretion rate is accurately described by the spherical model of Sect. 5:

$$\dot M_{\rm so} = \dot M_{\rm sph}(\mathcal{M}_\infty)\left[1+\mathcal{O}\left\{{\rm Max}(\bar r_{\rm so}-\bar r_0)^2\right\}\right] \ . \tag{103}$$

In order to approximate the mass accretion rate $\dot M_{\rm so}$, one must estimate the value of the effective Mach number $\mathcal{M}_{\rm e}$, the effective sonic radius $\bar r_{\rm so}(\theta_e)$ and the integral of $({\rm d}\Phi/4\pi r_{\rm so}^2)$. If the shock is detached, we can make simple guesses if the spherical sonic radius r_0 is smaller than the accretion radius r_A. We then use the spherical approximation for Φ and r_{so}, and use an ad-hoc expression for $\mathcal{M}_e$ only, to account for the asymmetry. We see from Fig. 4 that $r_0 < r_A$ for $5/3 > \gamma > 9/7$. The range $9/7 > \gamma > 1$, and especially the vicinity of $\gamma = 1$, requires a more careful treatment because r_0 can be orders of magnitude larger than r_A. Consequently, we restrict the present approach to the range $5/3 > \gamma > 9/7$, and make the simple approximation $\bar{r}_{so}(\theta_e) \sim \bar{r}_0$.

Since we would like to recover the Hoyle–Lyttleton accretion rate $\dot{M}_{HL}$ for high values of the Mach number, we see from Eq. (85) that this requires a constant value for the ratio $\mathcal{M}_e/\mathcal{M}_\infty$ when $\mathcal{M}_\infty \to \infty$. As a first approximation, we propose the ad–hoc prescription that $\dot{M}_{so} \to \lambda \dot{M}_{HL}$ when $\mathcal{M}_\infty \to \infty$, and retain the same ratio $\mathcal{M}_e/\mathcal{M}_\infty$ for intermediate values of $\mathcal{M}_\infty$. Neglecting the variations of the sound velocity before the shock, we can write the effective Mach number in terms of the angle φ_e of the "effective flow line" of entropy $S(\mathcal{M}_e)$ and the normal to the shock surface, and the distance r_e between the accretor and the intersection of this flow line with the shock surface:

$$\frac{\mathcal{M}_e}{\mathcal{M}_\infty} = \cos\varphi_e \left(1 + \frac{r_A}{r_e}\right)^{\frac{1}{2}} . \tag{104}$$

A geometrical interpretation is the following. Let the accretion radius r_A act as a scaling factor on the topology of the accreted flow, and keep the angle φ_e and the ratio r_A/r_e independent of the Mach number. Eq. (104) then implies that the ratio $\mathcal{M}_e/\mathcal{M}_\infty$ is constant. This does not contradict the fact that the opening angle of the Mach cone, well after the accretor, depends on the Mach number, since our approximation deals with the region of the bow shock which is mainly ahead of the accretor.

We obtain, for $\mathcal{M}_e \geq 1$:

$$\int_0^{\theta_{so}} \frac{d\Phi}{4\pi r_{so}^2} \sim 1 , \tag{105}$$

$$\bar{r}_{so}(\theta_e) \sim \bar{r}_0 , \tag{106}$$

$$\frac{\mathcal{M}_e}{\mathcal{M}_\infty} \sim \frac{1}{2^\gamma \lambda^{\frac{\gamma-1}{2}}} \left[\frac{2}{\gamma}\right]^{\frac{1}{2}} \frac{(\gamma+1)^{\frac{\gamma+1}{2}}}{(\gamma-1)^{\frac{5(\gamma-1)}{4}}(5-3\gamma)^{\frac{5-3\gamma}{4}}} . \tag{107}$$

With $\mathcal{M}_e$ defined by this relation if $\mathcal{M}_e \geq 1$, and $\mathcal{M}_e = 1$ otherwise, our interpolation formula follows from Eq. (102):

$$\dot{M}_I \equiv \dot{M}_B \left[1 + \frac{\gamma-1}{2}\mathcal{M}_\infty^2\right]^{\frac{5-3\gamma}{2(\gamma-1)}} \left[\frac{(\gamma+1)\mathcal{M}_e^2}{2+(\gamma-1)\mathcal{M}_e^2}\right]^{\frac{-\gamma}{\gamma-1}} \left[\frac{\gamma+1}{2\gamma\mathcal{M}_e^2-\gamma+1}\right]^{\frac{1}{\gamma-1}} . \tag{108}$$

We extend our rough approximation to the case $\gamma = 5/3$, neglecting the mass accreted in the subsonic region. We know from Sect. 4.6 that this corresponds to a small (but not zero) fraction of the total flux of mass.

The curves displayed in Fig. 9 and Fig. 10 show the mass accretion rates obtained with our interpolation formula $\dot{M}_I$, the Bondi–Hoyle interpolation formula $\dot{M}_{BH}$ and the results of numerical simulations (Ruffert 1994b, 1995; Ruffert & Arnett 1994). For $\gamma = 5/3$ our interpolation Eq. (108), in $\dot{M}_{BH}$ units, rises monotonously with Mach number (Fig. 9). The numerical results fit only marginally well. Note that the numerical simulations with $\gamma = 5/3$ give only an upper bound for the mass accretion rate, since the accretor is always larger than the spherical sonic radius. For $\gamma = 4/3$ (Fig. 10) a prominent maximum is apparent both on the interpolation formula and on the

Fig. 9. Comparison between our interpolation formula and the numerical simulations. Mass accretion rates are in $\dot{M}_{BH}$ units. The solid line corresponds to $\lambda = 1$, the dotted line to $\lambda = 0.5$. For $\gamma = 5/3$, the numerical simulations provide only upper bounds to the mass accretion rate of a point mass because the sonic surface is always attached to the accretor.

Fig. 10. Same as Fig. 9, but for $\gamma = 4/3$.

numerical results. Comparing Fig. 10 with the corresponding curve in the lower part of Fig. 8 gives an indication on the role played by non–sphericity in reducing the mass accretion rate.
Despite the considerable simplification of ignoring the geometrical term $\Phi(\theta)$ and keeping the ratio $\mathcal{M}_{\rm e}/\mathcal{M}_\infty$ independent of $\mathcal{M}_\infty$, these curves are in reasonable agreement with the numerical simulations for $\gamma = 4/3$ and $\gamma = 5/3$. Thus we expect this analytic formula to be relevant for the whole range $5/3 < \gamma < 9/7$.
Note that we do not solve the question of the dependence of the mass accretion rate with respect to the adiabatic index for high Mach numbers. For this purpose, and following Bondi & Hoyle (1944), we introduced the constant λ, assumed to be between 0.5 and 1. Our interpolation formula is nothing more than a natural way to link the Bondi mass accretion rate at $\mathcal{M}_\infty = 0$ with the Hoyle-Lyttleton mass accretion rate at $\mathcal{M}_\infty \to \infty$.
One should also keep in mind that the mass accretion rate obtained in the numerical simulations is for most models a time average over the fluctuations or quasi periodic oscillations due to the instability of the flow, and therefore differs from the exact mass accretion rate of the solution of the stationary equations. This instability is stronger for γ close to $5/3$.

7. Conclusions

By using a geometrical interpretation of the shape of the flux tube at the sonic radius, we have shown the particular significance of the radius r_0 (Eq. 33), which depends only on the adiabatic index and the energy of the flow. It is not only the sonic radius of all spherical flows, but is also related through the property $\mathcal{P}$ (Sect. 3.3) to the sonic surface of axisymmetric flows.
By reducing the stationary flow equations to a single partial differential equation, we have performed a local analysis near the accretor and have obtained some general results which aim at clarifying the diversity of possible configurations. We have extended the classification introduced by Bondi (1952) to axisymmetric stationary flows. In addition to the subsonic and supersonic types of accretion, angular sectors without any accretion are also possible, as well as singular directions of infinitely high accretion flux. This is illustrated by the self-similar solution found by Bisnovatyi-Kogan et al. (1979), which is a very particular singular case ($\theta_{\rm c} = 0$).
The angular sectors without any accretion is subsonic for flows with a detached shock, so that $\theta_{\rm so} \le \theta_{\rm c}$ in the notation introduced in Sect. 4.1.
Among some of the properties that we established for flows with $\gamma < 5/3$ are the following:
(i) the sonic surface is likely to be attached to the accretor for nearly isothermal flows with high Mach numbers,
(ii) isentropic accretion proceeds mostly from the downstream hemisphere of the accretor,
(iii) subsonic accretion must be isentropic.
We have also found a series of properties for flows with $\gamma = 5/3$:
(i) accretion is always regular,
(ii) the sonic surface is always attached to the accretor,
(iii) the pressure distribution is spherically symmetric to first order,
(iv) the Mach number and the entropy at a point like accretor are algebraically related to the local mass flux,
(v) shocked matter is accreted mostly from the downstream hemisphere, where the density, velocity and Mach number are maximum, and the temperature and entropy are minimum,
(vi) isentropic accretion is spherically symmetric to first order for the velocity, temperature, density, mass flux, and Mach number.

3–D numerical simulations have shown that the strongest instabilities occur with the adiabatic index $\gamma = 5/3$. The fact that subsonic regions invariably reach the accretor for $\gamma = 5/3$ might be considered as a warning about the possible role, in the instability mechanism, of the boundary conditions at the surface of the accretor. For $\gamma < 5/3$ and sufficiently small accretors, it would be interesting to check for the presence of the instability in cases where the accretor is surrounded by a supersonic region (Type F in the nomenclature of Sect. 3.1).

We have also determined the departure from sphericity, and constrained the radial variation of the angle β for $r \to 0$. In particular, we have stressed the influence of the entropy gradient on the bending of the flow lines for supersonic flows with $\gamma < 5/3$ and $\gamma = 5/3$.

We have stressed the role of the geometrical shape of the shock in the determination of the entropy of the accreted matter, and contrasted it with the simpler case of shocked spherical flows. In this latter case, we have shown the relevance of the entropy-energy approach, and noted that the mass accretion rate scales like the Hoyle–Lyttleton formula for high Mach numbers. Moreover, we have outlined the particularity of nearly isothermal flows for which the mass accretion rate can be a factor $2/(\gamma - 1)$ higher than the Bondi mass accretion rate, when the kinetic energy at infinity is comparable to the thermal energy. This demonstrates the fundamental difference of the BHL flows that have γ close to 1 and those with γ close to 5/3.
We have shown that the total mass accretion rate equals the mass accretion rate through the sonic surface, for shocked regular flows with $\gamma < 5/3$. We have derived an interpolation formula for the mass accretion rate valid in the range $9/7 < \gamma < 5/3$. It links spherical accretion to the case of highly supersonic accretion, with reasonable agreement with numerical simulations.

Analytical estimates of the following quantities, however, are still missing:
(i) the distance of the shock as a function of γ and $\mathcal{M}_\infty$,
(ii) the value of $\theta_{\rm so}$ and $\theta_{\rm c}$ as a function of γ and $\mathcal{M}_\infty$,
(iii) the mass accretion rate in the limit of infinite Mach numbers, as a function of γ.
Nevertheless, our classification will help perform, in a forthcoming paper, a local stability analysis of all the configurations considered.

Acknowledgements. TF was supported by the EC grant ERB-CHRX-CT93-0329, as part of the research network 'accretion onto compact objects and protostars'. We acknowledge useful comments by Dr. H. Spruit and Dr. U. Anzer.

A. Third order partial differential system for an axisymmetric stationary flow

The combined vorticity equation, continuity equation and entropy equation are written as functions of $\mathcal{M}, \beta, S$ as follows:

$$\begin{aligned}
&(1-\mathcal{M}^2\cos^2\beta)\frac{\partial\beta}{\partial\log r} - \mathcal{M}^2\sin\beta\cos\beta\frac{\partial\beta}{\partial\theta} = \\
&\frac{1-\mathcal{M}^2}{2+(\gamma-1)\mathcal{M}^2}\frac{\partial\log\mathcal{M}^2}{\partial\theta} + \frac{1-\mathcal{M}^2}{\gamma\mathcal{M}^2}\frac{\partial S}{\partial\theta} \\
&+\frac{\sin^2\beta}{\tan\theta} - \frac{\sin\beta\cos\beta}{1+\bar{r}}\left[\frac{2-\gamma}{\gamma-1} - \frac{1+2\bar{r}}{2}\mathcal{M}^2 - \bar{r}\right] , \qquad \text{(A1)}\\
&\frac{1-\mathcal{M}^2\cos^2\beta}{2+(\gamma-1)\mathcal{M}^2}\frac{\partial\log\mathcal{M}^2}{\partial\log r} - \frac{\mathcal{M}^2\sin\beta\cos\beta}{2+(\gamma-1)\mathcal{M}^2}\frac{\partial\log\mathcal{M}^2}{\partial\theta} = \\
&-\frac{\partial\beta}{\partial\theta} + \frac{\tan\beta}{\gamma\mathcal{M}^2}\frac{\partial S}{\partial\theta} + \frac{5-3\gamma-2(2-\gamma)\sin^2\beta}{2(1+\bar{r})(\gamma-1)} \\
&-\frac{\bar{r}}{1+\bar{r}}(2\cos^2\beta+1) - \frac{\sin\beta\cos\beta}{\tan\theta} , \qquad \text{(A2)}\\
&\frac{\partial S}{\partial\log r} = -\tan\beta\frac{\partial S}{\partial\theta} . \qquad \text{(A3)}
\end{aligned}$$

B. Proof of the property $\mathcal{P}$ of the axisymmetric sonic surface of Type F flows

Using the axisymmetry condition and some simple trigonometry, the variation of the cross–section Φ along the flow line can be written:

$$\frac{\partial\log\Phi}{\partial l}\frac{\partial l}{\partial\log r} = 2 + \frac{\tan\beta}{\tan\theta} + \frac{r}{\cos\beta}\frac{\partial\beta}{\partial\mathbf{n}} , \qquad \text{(B1)}$$

where $\beta(r,\theta)$ is defined by Eq. (11), and its derivative is taken in the direction $\mathbf{n}$ perpendicular to the flow line (oriented towards increasing θ). For $\beta = 0$ we recover the spherical case of conical flow tubes, with a cross section proportional to the square of the distance.
We can use Eq. (B1) along the detached sonic surface, together with Eq. (32), for $0 \le \theta \le \pi$:

$$\bar{r}_{\rm so} = \frac{\bar{r}_0 - f(\theta)}{1+f(\theta)} , \text{with} \qquad \text{(B2)}$$

$$f(\theta) \equiv \frac{1}{2}\left(\frac{r_{\rm so}}{\cos\beta}\frac{\partial\beta}{\partial\mathbf{n}} + \frac{\tan\beta}{\tan\theta}\right) . \qquad \text{(B3)}$$

Let us now prove that the sonic radius reaches the value of the spherical radius at least once, i.e. that $f(\theta)$ has to vanish.
Axisymmetry imposes $\beta(r,\theta=0) = \beta(r,\theta=\pi) = 0$, and by Eq. (B3):

$$f(0) = \frac{\partial\beta}{\partial\theta}(0) , \qquad \text{(B4)}$$

$$f(\pi) = \frac{\partial\beta}{\partial\theta}(\pi) . \qquad \text{(B5)}$$

Suppose, for example, that the sonic surface is inside the sphere of radius r_0 and detached from the accretor, i.e. $f(\theta) > \epsilon > 0$ for $\theta \in [0,\pi]$. Equations (B4) and (B5) imply that $\beta(r,\theta)$ is strictly positive near $r_{\rm so}(\theta=0)$, and strictly negative near $r_{\rm so}(\theta=\pi)$. A line must exist in the (r,θ) plane separating $r_{\rm so}(0)$ from $r_{\rm so}(\pi)$, along which β vanishes, when decreasing from a region of positive values to the region of negative values. We denote by $r_{\rm so}(\theta_{\rm i})$ the intersection of this line with the sonic surface:

$$f(\theta_{\rm i}) = \frac{1}{2}\left(\frac{r_{\rm so}}{\cos\beta}\frac{\partial\beta}{\partial\mathbf{n}}\right) \le 0 , \qquad \text{(B6)}$$

which contradicts the hypothesis. The same contradiction arises if we suppose that $f(\theta) < -\epsilon < 0$. Consequently f must vanish for some value of θ.

C. Linearized partial differential equation for $\gamma < 5/3$

By using Eq. (23), we can relate the second radial derivative of Ψ to its first radial derivative, at $r = 0$, through the following equation:

$$\lim_{\bar{r}\to 0}\left[\frac{\bar{r}^2\frac{\partial^2\Psi}{\partial\bar{r}^2}}{\bar{r}\frac{\partial\Psi}{\partial\bar{r}}}\right] = \lim_{\bar{r}\to 0}\left[\frac{\partial\log\beta}{\partial\log\bar{r}} - 1 + \bar{r}\frac{\partial^2\Psi}{\partial\bar{r}\partial\theta}\left(\frac{\partial\Psi}{\partial\theta}\right)^{-1}\right] . \qquad \text{(C1)}$$

The local mass flux is finite for regular flows, and therefore the limit when $r \to 0$ of $(\bar{r}\partial^2\Psi/\partial\bar{r}\partial\theta)$ is zero in the angular sectors where the flow is regular.
Let us define the new radial variable $z \equiv r^{(5-3\gamma)/2}$. Equation (26) implies to first order:

$$z\mathcal{M}^2 \sim \left(\frac{1}{\sin\theta}\frac{\partial\Psi_0}{\partial\theta}\right)^{1-\gamma} . \qquad \text{(C2)}$$

(i) If Eq. (56) is a strict inequality, Eq. (20) implies that the pressure is spherically symmetric to first order. Using Eqs. (38) and (52), the stream function $\Psi_0(\theta)$ at the surface of the accretor is directly related to the entropy $S_0(\theta)$ by:

$$\frac{\partial}{\partial\theta}\left[\left(\frac{1}{\sin\theta}\frac{\partial\Psi_0}{\partial\theta}\right)^{\gamma} {\rm e}^{-S_0}\right] = 0 . \qquad \text{(C3)}$$

The leading terms of the differential Eq. (27) satisfy the following equation:

$$\left\{(1+\epsilon_1)a\frac{\partial^2}{\partial\theta^2} + (1+\epsilon_2)b\frac{\partial}{\partial\theta} + (1+\epsilon_3)c + (1+\epsilon_4)z\frac{\partial^2}{\partial z^2} + \frac{3(2-\gamma)}{5-3\gamma}(1+\epsilon_5)\frac{\partial}{\partial z}\right\}\Psi_1 = (1+\epsilon_6)dz , \qquad \text{(C4)}$$

where the six functions $\epsilon_i(z,\theta)$ converge to zero when $z \to 0$. The functions a, b, c, d depend on θ only, and are defined as follows:

$$a \equiv -\left(\frac{2}{5-3\gamma}\right)^2\left(\frac{1}{\sin\theta}\frac{\partial\Psi_0}{\partial\theta}\right)^{\gamma-1} , \qquad \text{(C5)}$$

$$b \equiv \left(\frac{2}{5-3\gamma}\right)^2\left(\frac{1}{\sin\theta}\frac{\partial\Psi_0}{\partial\theta}\right)^{\gamma-1}\left(\frac{1}{\tan\theta} + 2\frac{\partial\Psi_0}{\partial\theta}\frac{S'(\Psi_0)}{\gamma}\right) , \qquad \text{(C6)}$$

$$c \equiv \left(\frac{2}{5-3\gamma}\right)^2\left(\frac{1}{\sin\theta}\frac{\partial\Psi_0}{\partial\theta}\right)^{\gamma-1}\left(\frac{\partial\Psi_0}{\partial\theta}\right)^2\frac{S''(\Psi_0)}{\gamma} , \qquad \text{(C7)}$$

$$d \equiv \left(\frac{2}{5-3\gamma}\right)^2\left(\frac{\partial\Psi_0}{\partial\theta}\right)^{2\gamma}\frac{S'(\Psi_0)}{\gamma(\sin\theta)^{2(\gamma-1)}} . \qquad \text{(C8)}$$

Assuming $\lim_{z\to 0}(\partial\log\Psi_1/\partial\log z) > 2$ and $d \neq 0$ contradicts Eq. (C4). Thus we conclude that:

$$\left(\frac{\partial\log\Psi_1}{\partial\log z}\right) \leq 2 \;\text{ for } S'(\Psi_0)\neq 0\ . \tag{C9}$$

By derivating Eq. (27) with respect to r and considering the leading terms, we find that $z\partial\Psi_1/\partial z$ satisfies the same Eq. (C4) as Ψ_1 does. Using Eq. (23), we obtain Eq. (57) for regular sectors with a non–uniform entropy.

(ii) If Eq. (56) is an equality, we use Eq. (C1) in order to write the first order terms of Eq. (27) as follows:

$$\lim_{z\to 0}\frac{\partial\Psi}{\partial z} = \frac{4\mathrm{e}^{S_0}\sin\theta}{3\gamma(5-3\gamma)(2-\gamma)}\frac{\partial}{\partial\theta}\left[\left(\frac{1}{\sin\theta}\frac{\partial\Psi_0}{\partial\theta}\right)^{\gamma}\mathrm{e}^{-S_0}\right]\ . \tag{C10}$$

In both cases (i) and (ii), S_0, Ψ_0 and the radial derivative $(\partial\Psi/\partial z)_0$ cease to be a set of three free functions of θ on the surface of the accretor, when the accretor size decreases to zero. Let us recall that for spherical flows, one parameter (the mass flux) is required as boundary condition on the surface $r = r_\star$ of the accretor, with no particular change if $r_\star \to 0$. In this respect, the differential system (27) is more singular at $r = 0$ for axisymmetric flows than for spherical flows.

D. Linearized partial differential equation for $\gamma = 5/3$

Because the stream function Ψ is finite everywhere, ϵ_Ψ and $\bar{r}^2\partial^2\Psi/\partial\bar{r}^2$ tend to zero with decreasing $\bar{r}$. Eq. (26) implies that when $\gamma = 5/3$, the Mach number tends to a finite limit everywhere where the local mass flux (i.e. $\partial\Psi_0/\partial\theta$ according to Eq. (38)) is not zero. Taking the limit of Eq. (27) when $\bar{r} \to 0$, we find that its last term must vanish at $\bar{r} = 0$:

$$\frac{1}{\tan\theta}\frac{\partial\Psi_0}{\partial\theta} - \frac{\partial^2\Psi_0}{\partial\theta^2} + \left(\frac{\partial\Psi_0}{\partial\theta}\right)^2\left(1-\frac{1}{\mathcal{M}_0^2}\right)\frac{3S'(\Psi_0)}{5} = 0\ , \tag{D1}$$

where the subscript 0 denotes the value of the function at $r = 0$. This equation is equivalent to the condition that the pressure is spherically symmetric to first order.

In order to find the behaviour of the quantities $\Psi, \mathcal{M}^2$ near $\bar{r} = 0$, we consider only the leading terms of Eqs. (26) and (27). We first define $\mathcal{M}_1$ and Ψ_1 as follows:

$$\mathcal{M}^2(r,\theta) \equiv \mathcal{M}_0^2(\theta)(1+\mathcal{M}_1(r,\theta))\ , \tag{D2}$$
$$\Psi(r,\theta) \equiv \Psi_0(\theta)+\Psi_1(r,\theta)\ . \tag{D3}$$

By linearizing Eq. (26) near $\mathcal{M}_0^2 \neq 1$, we obtain to first order:

$$\mathcal{M}_1 \sim \frac{4}{3}\frac{3+\mathcal{M}_0^2}{1-\mathcal{M}_0^2}\left[-\bar{r}+\frac{(3+\mathcal{M}_0^2)^4}{2\mathcal{M}_0^2\sin^2\theta}\frac{\partial\Psi_0}{\partial\theta}\frac{\partial\Psi_1}{\partial\theta}\right]\ . \tag{D4}$$

Introducing this into Eq. (27), we obtain the following leading terms:

$$\left\{(1+\epsilon_7)e\frac{\partial^2}{\partial\theta^2}+(1+\epsilon_8)f\frac{\partial}{\partial\theta}+(1+\epsilon_9)g + (1+\epsilon_{10})\bar{r}^2\frac{\partial^2}{\partial\bar{r}^2}+\frac{3}{2}(1+\epsilon_{11})\bar{r}\frac{\partial}{\partial\bar{r}}\right\}\Psi_1 = (1+\epsilon_{12})h\bar{r}\ , \tag{D5}$$

where the six functions $\epsilon_j(\bar{r},\theta)$ converge to zero when $\bar{r}\to 0$. The functions e, f, g, h depend on θ only, and are defined as follows:

$$e \equiv \frac{1}{1-\mathcal{M}_0^2}\ , \tag{D6}$$

$$f \equiv -\frac{1}{1-\mathcal{M}_0^2}\frac{1}{\tan\theta} - 6\,\frac{\partial\Psi_0}{\partial\theta}\frac{S'(\Psi_0)}{5\mathcal{M}_0^2}\left[\frac{(3+\mathcal{M}_0^2)^5}{3\mathcal{M}_0^2(1-\mathcal{M}_0^2)^2\sin^2\theta}\left(\frac{\partial\Psi_0}{\partial\theta}\right)^2-1\right]\ , \tag{D7}$$

$$g \equiv \left(\frac{\partial\Psi_0}{\partial\theta}\right)^2\frac{3S''(\Psi_0)}{5\mathcal{M}_0^2}\ , \tag{D8}$$

$$h \equiv -\frac{4}{5}\frac{3+\mathcal{M}_0^2}{(1-\mathcal{M}_0^2)^2}\left(\frac{\partial\Psi_0}{\partial\theta}\right)^2\frac{S'(\Psi_0)}{\mathcal{M}_0^2}\ . \tag{D9}$$

Let us suppose that l is a positive number such that

$$\lim_{r\to 0}\frac{\partial\log\Psi_1}{\partial\log r} = 1+l > 1\ . \tag{D10}$$

If the entropy is not uniform ($h \neq 0$), the first two terms of Eq. (D5) are negligible compared to the rhs term. Dividing the remaining equation by $\bar{r}$, we obtain:

$$\left\{(1+\epsilon_7)e\frac{\partial^2}{\partial\theta^2}+(1+\epsilon_8)f\frac{\partial}{\partial\theta}+(1+\epsilon_9)g\right\}\frac{\Psi_1}{\bar{r}} = (1+\epsilon_{12})h\ . \tag{D11}$$

According to Eq. (D10), $\lim_{r\to 0}\Psi_1/\bar{r} = 0$. Thus Eq. (D11) contradicts our hypothesis (D10), and we conclude that if $h \neq 0$,

$$0 \leq \left(\lim_{r\to 0}\frac{\partial\log\Psi_1}{\partial\log r}\right) \leq 1\ . \tag{D12}$$

By derivating Eq. (27) with respect to $\bar{r}$, and keeping the leading terms, $\bar{r}\partial\Psi_1/\partial\bar{r}$ satisfies exactly the same equation (D5) as Ψ_1 does. From the same reasoning, we conclude that

$$0 \leq \left(\lim_{r\to 0}\frac{\partial\log}{\partial\log r}\frac{\partial\Psi_1}{\partial\log\bar{r}}\right) \leq 1\ . \tag{D13}$$

This lower bound on the scaling of $\bar{r}\partial\Psi_1/\partial\bar{r}$ is also a lower bound on the scaling of β: we obtain Eq. (71) by using Eqs. (23), (D13) and the regularity of the flow for $\gamma = 5/3$.

E. Approximation of the orbits within the supersonic region by hyperbolae

We check the validity of neglecting the pressure forces in the supersonic flow ahead of the shock, and assuming that the sound velocity is uniformly constant to its value at infinity c_∞. The velocity of the supersonic incoming gas is then defined by the unique hyperbolic trajectory passing trough this point, with velocity at infinity v_∞.

For each point (r,θ) of the shock surface, we can compute numerically the dimensionless impact parameter $\hat{a}$ (normalized to the accretion radius $r_{\rm A}$) of this hyperbola:

$$\hat{r} = \frac{2\hat{a}^2}{1+(1+4\hat{a}^2)^{1/2}\cos(\theta-\theta_\infty)}\ . \tag{E1}$$

The half angle θ_∞ of the hyperbola is defined by

$$\cos\theta_\infty = \frac{1}{(1+4\hat{a}^2)^{1/2}}\ . \tag{E2}$$

Let us calculate the variation of density along the axis of symmetry, due to both the compression by gravitational convergence of the hyperbolic trajectories and the dilation due to acceleration. This can be done using the continuity equation (2) in cylindrical coordinates, along the axis, for $\theta \to \pi$:

$$\frac{\partial \rho \hat{r}^2 v_r}{\partial \hat{r}} + 2\rho\hat{r}\frac{\partial v_\theta}{\partial \theta} = 0 \; . \tag{E3}$$

The azimuthal derivative of the azimuthal component of the velocity is directly related to the impact parameter a through the conservation of angular momentum, while the (negative) radial component of the velocity, along the axis, is given by the conservation of energy:

$$\hat{r}v_\theta \;=\; -\hat{a}v_\infty \;, \tag{E4}$$

$$v_r(\theta=\pi) \;=\; -v_\infty\left(1+\frac{1}{\hat{r}}\right)^{\frac{1}{2}} \; . \tag{E5}$$

In order to determine the azimuthal dependence of the impact parameter, let us consider the trajectories defined by Eq. (E1) for $(\theta-\pi) \to 0$. Since $a(\pi) = 0$, we write:

$$\hat{a}(\theta) = (\theta-\pi)\frac{\partial \hat{a}}{\partial \theta}(\pi) + \mathcal{O}\left((\theta-\pi)^3\right) \; . \tag{E6}$$

From first order expansions of Eq. (E2) and Eq. (E1), we find, for $(\theta-\pi) \to 0$:

$$\left(\frac{\partial \hat{a}}{\partial \theta}\right)^2 + \hat{r}\frac{\partial \hat{a}}{\partial \theta} - \frac{\hat{r}}{4} = 0 \; . \tag{E7}$$

Choosing the negative solution of this equation ($\hat{a}$ is positive and decreases to zero when θ increases to π), leads to:

$$\frac{\partial v_\theta}{\partial \theta}(\pi) = \frac{v_\infty}{2}\left[1+\left(1+\frac{1}{\hat{r}}\right)^{\frac{1}{2}}\right] \; . \tag{E8}$$

Using Eqs. (E8) and (E5) in Eq. (E3) we obtain:

$$\frac{\partial \log \rho}{\partial \hat{r}}(\pi) = \frac{1}{\hat{r}^{\frac{1}{2}}(\hat{r}+1)^{\frac{1}{2}}} - \frac{1}{2}\frac{1+2\hat{r}}{\hat{r}(1+\hat{r})} \; . \tag{E9}$$

This can be integrated to obtain the radial dependence of the density along the axis of symmetry:

$$\frac{\rho}{\rho_\infty}(\pi) = \frac{1}{2} + \frac{2+\frac{1}{\hat{r}}}{4\left(1+\frac{1}{\hat{r}}\right)^{1/2}} \; . \tag{E10}$$

The compression effect due to the convergence of the flow lines is consequently stronger than the dilatation due to the acceleration of the flow.
If the shock is not too close to the accretor, gravitational focusing is negligible and the density and temperature can be approximated as constant in the upstream supersonic flow. One can check from Eq. (E10) that this density enhancement is smaller than a factor of two for $\hat{r} > 0.03$. Note that when the shock is detached, its distance is generally of order $\hat{r}_{\rm sh}(\pi) \sim 0.2$ in numerical simulations. We deduce from Eq. (E10) that the sound velocity scales like $\hat{r}^{(\gamma-1)/2}$ when $\hat{r} \to 0$, and is therefore always negligible compared to the gravitational potential scaling like $\hat{r}^{-1}$.

F. Entropy gradient produced by a detached shock in the vicinity of the axis of symmetry

Let $(x_{\rm sh}, y_{\rm sh})$ be local coordinates in a frame chosen in a way such that $x_{\rm sh}$ is perpendicular to the shock surface, and $y_{\rm sh}$ is parallel to it. Let us call $\mathcal{M}_1$ the Mach number relative to the component of the velocity, ahead of and perpendicular to the shock surface. In our local system of coordinates,

$$\mathcal{M}_1 = \frac{v_{x1}}{c_1} \; . \tag{F1}$$

We shall use the classical convention of using the index "1" for quantities ahead of the shock, and the index "2" for quantities just after the shock.
We write the entropy gradient after the shock as:

$$\nabla S = \frac{v_2}{v_{x2}}\frac{\partial S_2}{\partial y} = \frac{v_2}{v_{x2}}\frac{\partial S_2}{\partial \mathcal{M}_1}\frac{\partial \mathcal{M}_1}{\partial y} \; . \tag{F2}$$

We can use the classical jump conditions (83) to express the entropy gradient as a function of $\mathcal{M}_1$ only:

$$\nabla S \;=\; \frac{v_2}{v_{x2}}\frac{2\eta}{\gamma-1}\frac{\partial \log \mathcal{M}_1}{\partial y} \;, \text{ where} \tag{F3}$$

$$\eta(\mathcal{M}_1) \;\equiv\; \frac{2\gamma(\gamma-1)(\mathcal{M}_1^2-1)^2}{(2+(\gamma-1)\mathcal{M}_1^2)(2\gamma\mathcal{M}_1^2-(\gamma-1))} < 1 \tag{F4}$$

We obtain v_{x1} by the vector product of the velocity and the vector tangent to the shock surface. Let the supersonic flow before the shock be described in cylindrical coordinates by the flow velocity $v_r(\hat{r},\theta), v_\theta(\hat{r},\theta)$. For the sake of clarity, we denote the velocity along the shock surface $r_{\rm sh}(\theta)$ by $v(\theta) \equiv v(\hat{r}_{\rm sh}(\theta),\theta)$ and a dot stands for the derivative with respect to the angle θ:

$$v_{x1}(\theta) \equiv \frac{\hat{r}_{\rm sh}(\theta)v_r(\theta) - \dot{\hat{r}}_{\rm sh}(\theta)v_\theta(\theta)}{\left(\hat{r}_{\rm sh}^2(\theta)+\dot{\hat{r}}_{\rm sh}^2(\theta)\right)^{\frac{1}{2}}} \; . \tag{F5}$$

We now prove that a regular axisymmetric shock surface cannot produce a local region of uniform entropy behind it, and more precisely, that the gradient of entropy created by the shock scales like the square of the azimuthal angle $(\theta-\pi)$ in the vicinity of the axis, for any shape of the shock which is regular and symmetric.
When not specified, the quantities are taken at $\theta = \pi$ in what follows. We also define $v_{\rm sh} \equiv v_r(\pi)$ and $\hat{r} \equiv \hat{r}_{\rm sh}(\pi)$. The symmetry condition imposes:

$$\dot{\hat{r}}_{\rm sh}(\pi) = 0 \tag{F6}$$

Using the symmetry of the problem, we make the following expansions for small values of $(\theta-\pi)$:

$$v_r(\theta) \;=\; v_{\rm sh} + \frac{(\theta-\pi)^2}{2}\left(\ddot{\hat{r}}_{\rm sh}\frac{\partial v_r}{\partial \hat{r}} + \frac{\partial^2 v_r}{\partial \theta^2}\right) + \mathcal{O}\left((\theta-\pi)^4\right) \;, \tag{F7}$$

$$v_\theta(\theta) \;=\; (\theta-\pi)\frac{\partial v_\theta}{\partial \theta} + \mathcal{O}\left((\theta-\pi)^3\right) \;, \tag{F8}$$

$$\hat{r}_{\rm sh}(\theta) \;=\; \hat{r}_{\rm sh} + \frac{(\theta-\pi)^2}{2}\ddot{\hat{r}}_{\rm sh} + \mathcal{O}\left((\theta-\pi)^4\right) \; . \tag{F9}$$

Using the expansions (F7), (F8), and (F9), we obtain:

$$\frac{v_{x1}(\theta)}{v_{\rm sh}} = 1 - \frac{(\theta-\pi)^2}{2}\left[\left(\frac{\ddot{\hat{r}}_{\rm sh}}{\hat{r}_{\rm sh}}\right)^2 + \frac{\ddot{\hat{r}}_{\rm sh}}{\hat{r}_{\rm sh}}\left(\frac{2}{v_{\rm sh}}\frac{\partial v_\theta}{\partial\theta} - \frac{\hat{r}_{\rm sh}}{v_{\rm sh}}\frac{\partial v_r}{\partial\hat{r}}\right) - \frac{1}{v_{\rm sh}}\frac{\partial^2 v_r}{\partial\theta^2}\right] + \mathcal{O}\left((\theta-\pi)^4\right) \ . \tag{F10}$$

In order to evaluate this expression, we use the approximation of the supersonic flow $v_r(\hat{r},\theta), v_\theta(\hat{r},\theta)$ by hyperbolic trajectories. Derivating the Bernoulli Eq. (7) with respect to $\hat{r}$ and θ, we obtain for $\theta=\pi$:

$$\frac{\partial^2 v_r}{\partial\theta^2} = -\frac{1}{v_{\rm sh}}\left(\frac{\partial v_\theta}{\partial\theta}\right)^2 \ , \tag{F11}$$

$$\frac{\partial v_r}{\partial\hat{r}} = -\frac{v_\infty^2}{2v_{\rm sh}\hat{r}_{\rm sh}^2} \ . \tag{F12}$$

Replacing these expressions, together with Eqs. (E5) and (E8) into Eq (F10), the effective Mach number is:

$$\frac{\mathcal{M}_1(\theta)}{\mathcal{M}_1(\pi)} = 1 - \frac{(\theta-\pi)^2}{2}\left[\frac{3+4\hat{r}_{\rm sh}+4\hat{r}_{\rm sh}^{\frac{1}{2}}(1+\hat{r}_{\rm sh})^{\frac{1}{2}}}{16\hat{r}_{\rm sh}(1+\hat{r}_{\rm sh})^2} + C^2\right] + \mathcal{O}\left((\theta-\pi)^4\right) \ , \tag{F13}$$

where the positive contribution C^2 depends on the second derivative $\ddot{\hat{r}}_{\rm sh}(\pi)$ of the shock surface on the symmetry axis, and is defined as:

$$C \equiv \frac{\ddot{\hat{r}}_{\rm sh}}{\hat{r}_{\rm sh}} + \frac{1}{v_{\rm sh}}\left(\frac{\partial v_\theta}{\partial\theta} - \frac{\hat{r}_{\rm sh}}{2}\frac{\partial v_r}{\partial\hat{r}}\right) \tag{F14}$$

We conclude that *for any shape of the detached shock surface*, the effective Mach number near the symmetry axis decreases at least as the square of the azimuthal angle $(\theta-\pi)^2$.

This result is particularly useful in order to prove that the mass accretion rate in the subsonic region of Type SF flows decreases to zero with the size of the accretor.

References

Bisnovatyi-Kogan G.S., Kazhdan Y.M., Klypin A.A., Lustkii A.E., Shakura N.I., 1979, SvA 23, 201

Boffin H.M.J., 1991, IAU Symp. 151

Bondi H., 1952, MNRAS 112, 195

Bondi H., Hoyle F., 1944, MNRAS 104, 273

Blondin J.M., 1994, *AIP Conf. Proc.* 308, 578, "The Evolution of X-ray Binaries", S.S. Holt and C.S. Day, eds.

Crocco L., 1936, Atti Reale Acc. Naz. Lincei 23, 115; cited in Courant & Friedrichs, *Supersonic Flow and Shock Waves*, Springer, New York, 1948

Eadie G., Peacock A., Pounds K.A., Watson M., 1975, MNRAS 172, 35P

Eddington A.S., 1926, *The Internal Constitution of the Stars*, Cambridge University Press, Cambridge Classics Series 1988

Fryxell B.A., Taam R.E., 1988, ApJ 335, 862

Hoyle F., Lyttleton R.A., 1939, *Proc. Cam. Phil. Soc.* 35, 405

Hunt R., 1971, MNRAS 154, 141

Hunt R., 1979, MNRAS 188, 83

Ishii T., Matsuda T., Shima E., Livio M., Anzer U., Börner G., 1993, ApJ 404, 706

Landau L.D., Lifshitz E.M., 1987, *Fluid Mechanics*, Vol. 6, Pergamon Press

Matsuda T., Sekino N., Sawada K., Shima E., Livio M., Anzer U., Börner G., 1991, A&A 248, 301

Matsuda T., Ishii T., Sekino N., Sawada K., Shima E., Livio M., Anzer U., 1992, MNRAS 255, 183

Ruffert M., 1992, A&A 265, 82

Ruffert M., 1994a, ApJ 427, 342

Ruffert M., 1994b, A&AS 106, 505

Ruffert M., 1995, A&AS 113, 133

Ruffert M., 1996, A&A, in press

Ruffert M., Arnett D., 1994, ApJ 427, 351

Ruffert M., Melia F., 1994, A&A 288, L29

Shima E., Matsuda T., Takeda H., Sawada K., 1985, MNRAS 217, 367

Theuns T., David M., 1992, ApJ 384, 587

Theuns T., Boffin H.M.J, Jorissen A., 1996, A&A, in press

This article was processed by the author using Springer-Verlag LaTeX A&A style file *L-AA* version 3.

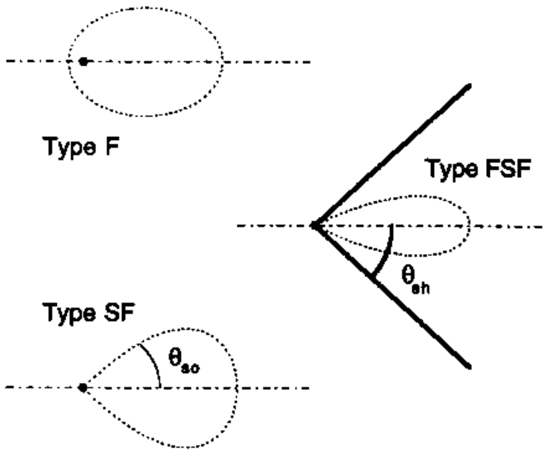

Figure 1.

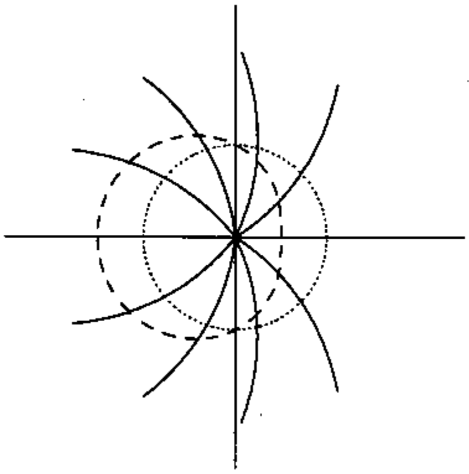

Figure 3.

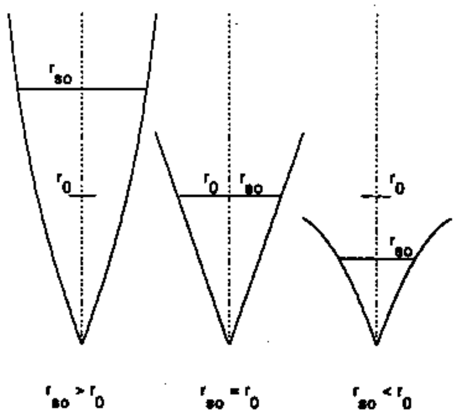

Figure 2.

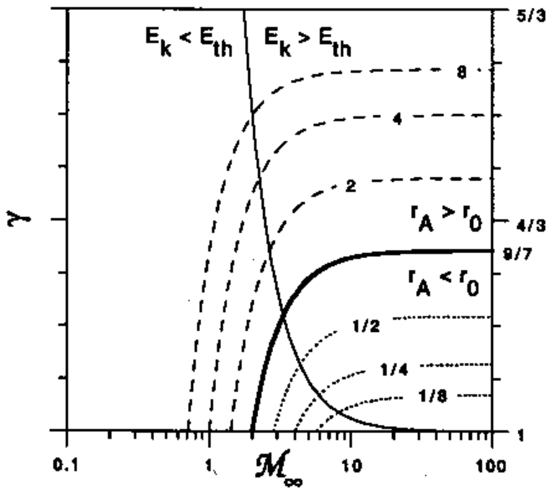

Figure 4.

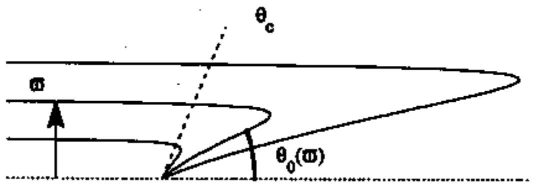

Figure 5.

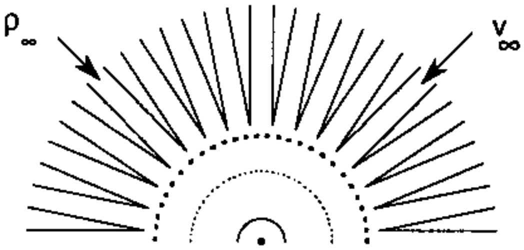

Figure 6.

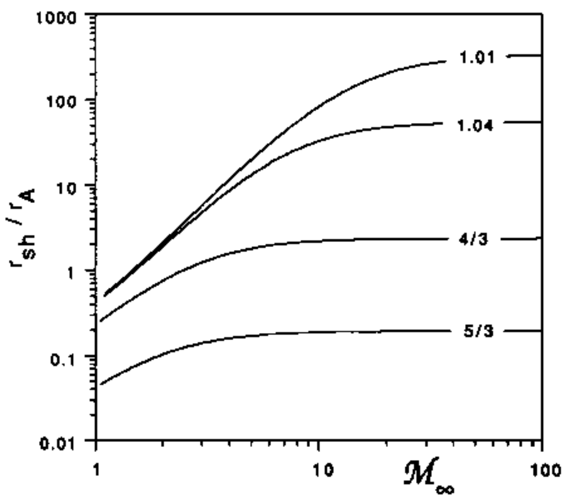

Figure 7.

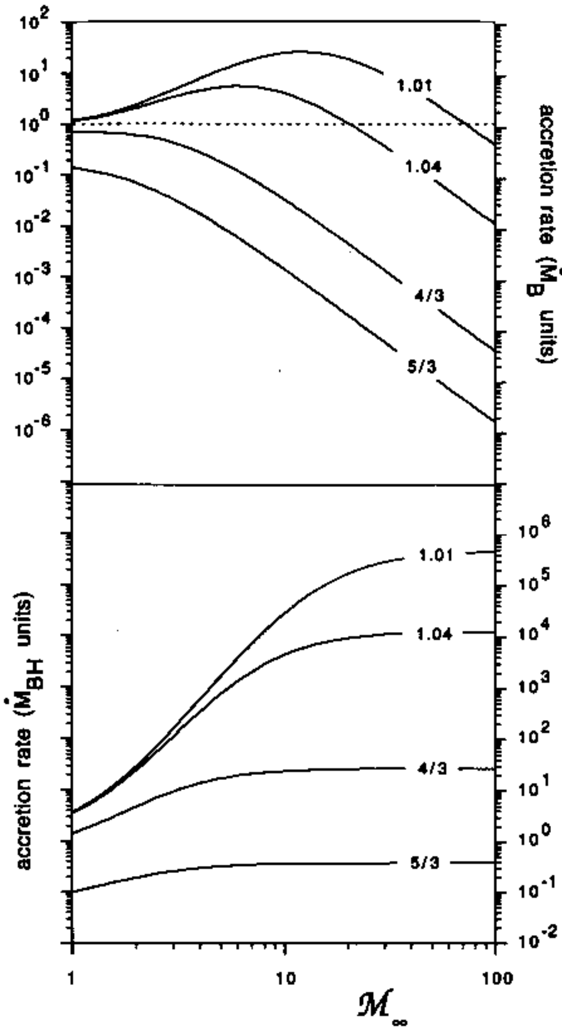

Figure 8.

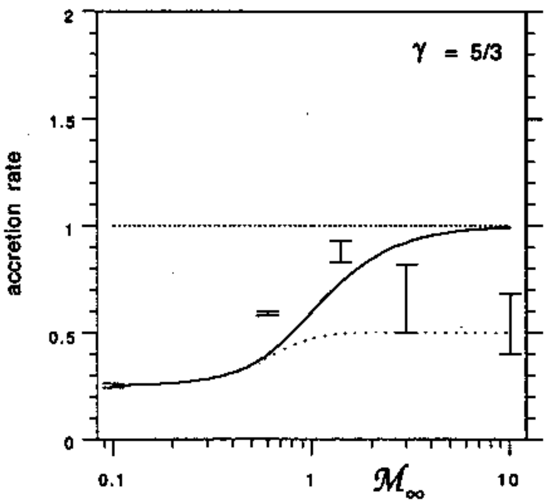

Figure 9.

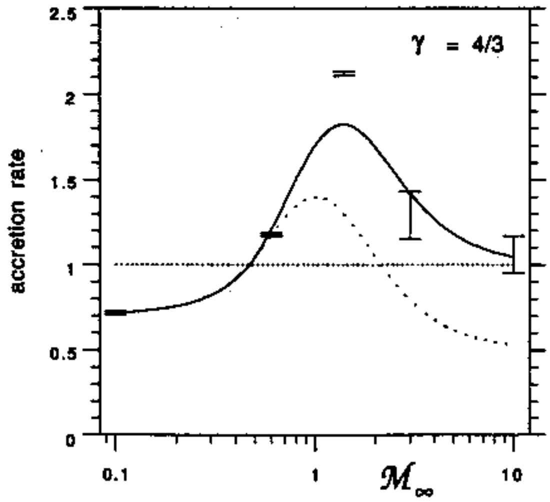

Figure 10.